UNIVERSITY of York

This is a repository copy of *Reactive Oxygen Species Regulate Activity-Dependent Neuronal Plasticity in Drosophila*.

White Rose Research Online URL for this paper:
https://eprints.whiterose.ac.uk/140146/

Version: Accepted Version

Article:
Oswald, Matthew Charles William, Brooks, Paul S., Zwart, Maarten F. et al. (7 more authors) (2018) Reactive Oxygen Species Regulate Activity-Dependent Neuronal Plasticity in Drosophila. eLife. e39393. ISSN 2050-084X

https://doi.org/10.7554/eLife.39393

Reuse
This article is distributed under the terms of the Creative Commons Attribution (CC BY) licence. This licence allows you to distribute, remix, tweak, and build upon the work, even commercially, as long as you credit the authors for the original work. More information and the full terms of the licence here: https://creativecommons.org/licenses/

Takedown
If you consider content in White Rose Research Online to be in breach of UK law, please notify us by emailing eprints@whiterose.ac.uk including the URL of the record and the reason for the withdrawal request.

White Rose
university consortium
Universities of Leeds, Sheffield & York

eprints@whiterose.ac.uk
https://eprints.whiterose.ac.uk/

Title: Reactive Oxygen Species Regulate Activity-Dependent Neuronal Plasticity in *Drosophila*

Authors: Matthew C. W. Oswald[1*], Paul S. Brooks[1], Maarten F. Zwart[2], Amrita Mukherjee[1], Ryan J. H. West[3,4], Carlo Giachello[3], Khomgrit Morarach[1], Richard A. Baines[3], Sean T. Sweeney[4], Matthias Landgraf[1*]

*Correspondence to: mo364@cam.ac.uk and ml10006@cam.ac.uk

Affiliations:

[1] University of Cambridge, Department of Zoology, Downing Street, Cambridge, CB2 3EJ, United Kingdom

[2] HHMI Janelia Research Campus, Ashburn, VA, 20147, USA

[3] Faculty of Biology, Medicine and Health, University of Manchester, Oxford Road, Manchester, M13 9PT, UK

[4] Department of Biology, University of York, Heslington York YO10 5DD, United Kingdom

Abstract:

Reactive oxygen species (ROS) have been extensively studied as damaging agents associated with ageing and neurodegenerative conditions. Their role in the nervous system under non-pathological conditions has remained poorly understood. Working with the *Drosophila* larval locomotor network, we show that in neurons ROS act as obligate signals required for neuronal activity-dependent structural plasticity, of both pre- and postsynaptic terminals. ROS signaling is also necessary for maintaining evoked synaptic transmission at the neuromuscular junction, and for activity-regulated homeostatic adjustment of motor network output, as measured by larval crawling behavior. We identified the highly conserved Parkinson's disease-linked protein DJ-1ß as a redox sensor in neurons where it regulates structural plasticity, in part via modulation of the PTEN-PI3Kinase pathway. This study provides a new conceptual framework of neuronal ROS as second messengers required for neuronal plasticity and for network tuning, whose dysregulation in the ageing brain and under neurodegenerative conditions may contribute to synaptic dysfunction.

35
36
37 **Introduction**
38
39 Levels of reactive oxygen species (ROS) in the brain increase with ageing and high levels of ROS are a
40 hallmark of neurodegeneration, including Alzheimer's and Parkinson's disease (Höhn and Grune,
41 2013; Martins et al., 1986; Spina and Cohen, 1989) for review see (Milton and Sweeney, 2012).
42 Mitochondria are a significant source of ROS, which form as obligate byproducts of respiratory ATP
43 synthesis by 'leakage' of the electron transport chain, thus leading to the generation of superoxide
44 anions (O_2^-) and hydrogen peroxide (H_2O_2) (Halliwell, 1992). Implicit in their name, ROS are highly
45 reactive, containing one or more unpaired electrons, with the potential to modify and damage by
46 oxidation proteins, lipids and DNA (Gladyshev, 2014; Harman, 1956; Stuart et al., 2014). Importantly,
47 ROS have also been recognized as signaling molecules in metabolic pathways (Liemburg-Apers et al.,
48 2015) and controlling the activity of transcription factors such as AP-1 and Nrf2 (Jindra et al., 2004;
49 Soriano et al., 2009). Moreover, several kinase signaling pathways are enhanced by ROS, either by
50 oxidation of kinase interacting modulators, such as thioredoxin or glutathione-S-transferases (Adler
51 et al., 1999; Saitoh et al., 1998), or through inhibition of counteracting phosphatases, e.g. PTEN, by
52 oxidation of the active site cysteine residue (Finkel, 2011; Stuart et al., 2014; Tonks, 2005).
53 We previously showed in a model for lysosomal storage diseases that ROS can regulate
54 neuromuscular junction (NMJ) structure (Milton et al., 2011). NMDA receptor stimulation can lead
55 to ROS generation (Bindokas et al., 1996; Brennan et al., 2009; Dugan et al., 1995), and in
56 hippocampal and spinal cord slices ROS have been shown sufficient and necessary for inducing
57 'Hebbian' forms of plasticity (LTP) (Kamsler and Segal, 2003a; Kamsler and Segal, 2003b; Klann,
58 1998; Knapp and Klann, 2002; Lee et al., 2010). Conversely, disturbing the ROS balance by over-
59 expression of the scavenger superoxide dismutase caused defects in hippocampal LTP and learning
60 paradigms in mice (Gahtan et al., 1998; Levin et al., 1998; Thiels et al., 2000). Recent studies have
61 linked increased ROS levels with neurodevelopmental conditions such as schizophrenia, bipolar and
62 autism spectrum disorders (Do et al., 2015; Steullet et al., 2017).
63 Here, we set out to investigate potential roles for ROS in the nervous system under non-
64 pathological conditions, which are much less well understood. The brain is arguably the most energy
65 demanding organ and mitochondrial oxidative phosphorylation is a major source of ROS (Attwell and
66 Laughlin, 2001; Hallermann et al., 2012; Zhu et al., 2012). We therefore asked whether neurons
67 might utilize mitochondrial metabolic ROS as feedback signals to mediate activity-regulated changes.
68 As an experimental model we used the motor system of the fruitfly larva, *Drosophila melanogaster*,
69 which allows access to uniquely identifiable motoneurons in the ventral nerve cord and their specific
70 body wall target muscles (Kohsaka et al., 2012). We established an experimental paradigm for
71 studying activity-regulated structural adjustments across an identified motoneuron, quantifying
72 changes at both pre- and postsynaptic terminals. We show that thermogenetic neuronal over-
73 activation leads to the generation of ROS at presynaptic terminals, and that ROS signaling is
74 necessary and sufficient for the activity-regulated structural adjustments. As a cellular ROS sensor
75 we identified the conserved redox sensitive protein DJ-1ß, a homologue of vertebrate DJ-1 (PARK7)
76 (Meulener et al., 2005), and the phosphatase and tensin homolog (PTEN) and PI3kinase as
77 downstream effectors of activity-ROS-mediated structural plasticity. We find that ROS signaling is

78 also required for maintaining constancy of evoked transmission at the neuromuscular junction (NMJ)
79 with a separate ROS pathway regulating the amplitude of spontaneous vesicle release events.
80 Behaviourally, ROS signaling is required for the motor network to adjust homeostatically to return to
81 a set crawling speed following prolonged overactivation.
82 In summary, this study establishes a new framework for studying ROS in the nervous system:
83 as obligatory regulators that inform neurons about their activation status, and as obligatory
84 mediators of activity-induced plasticity, both structural and physiological.
85
86
87
88 **Results**
89
90 **Structural plasticity of synaptic terminals is regulated by neuronal activity**
91 Our aim was to explore roles for activity-regulated ROS signaling in the nervous system under non-
92 pathological conditions. Working with the *Drosophila* larval neuromuscular system allowed us to
93 target manipulations to identified nerve cells *in vivo* that manifest structural and functional plasticity
94 (Frank et al., 2013; Tripodi et al., 2008; Wolfram and Baines, 2013; Zwart et al., 2013). We focused
95 on two well characterized motoneurons, 'aCC' and 'RP2', which jointly innervate the dorsal acute
96 muscle 1 (DA1) (Figure 1A) (Baines et al., 1999; Baines et al., 2001; Bate, 1993; Choi et al., 2004;
97 Hoang and Chiba, 2001; Landgraf et al., 2003; Sink and Whitington, 1991). First, we characterized
98 activity-regulated morphological changes at the presynaptic neuromuscular junction (NMJ) and, in
99 the central nervous system (CNS), the branched postsynaptic dendritic arbors that receive input
100 from premotor interneurons (Baines et al., 1999; Schneider-Mizell et al., 2016; Zwart et al., 2013). A
101 simple method for increasing activity in the larval locomotor network is to increase ambient
102 temperature from the default standard of 25°C to 29°C or 32°C. Sigrist et al. (2003) and Zhong and
103 Wu (2004) previously demonstrated this to trigger increased locomotor activity and to result in
104 increased varicosity (bouton) number at presynaptic NMJs (Sigrist et al., 2003; Zhong and Wu, 2004).
105 We were able to reproduce and extend these findings: rearing larvae at higher ambient
106 temperatures results in NMJs having more boutons than controls by the third instar wandering
107 stage, 100 hrs after larval hatching (ALH) (grey data in Figure 1B-C, compare 25°C with 29°C and 32°C
108 conditions). To complement these systemic manipulations and to exclude potential non-specific
109 effects we turned to a cell-specific activation paradigm of selectively overactivating the aCC and RP2
110 motoneurons via targeted mis-expression of the warmth-gated cation channel dTrpA1. Expression of
111 dTrpA1 in neurons is a well established method for temperature controlled neuronal overactivation
112 (Hamada et al., 2008; Owald et al., 2015). For larval motoneurons in particular, Pulver and
113 colleagues demonstrated that dTrpA1 is activated above 24°C, at 25°C leading to action potential
114 firing frequencies of 9-12 Hz (moderate activation) and 22-30 Hz at 27°C (stronger activation) (Pulver
115 et al., 2009). These activation levels are within the physiological range of larval motoneurons,
116 thought to operate at approximately 42 Hz during muscle contraction cycles (Chouhan et al., 2010).
117 Similar to the systemic manipulations, we found that cell-specific thermogenetic dTrpA1 activation
118 of single motoneurons also led to titratable increases in bouton number at presynaptic NMJs (blue
119 data in Figure 1B-C). Note that these cell-specific dTrpA1-mediated activity manipulations were

120 carried out at 25°C and 27°C, sufficient to activate dTrpA1 expressing neurons, but otherwise not
121 causing significant changes in NMJ morphology in non-expressing motoneurons (Tsai et al., 2012).
122 Next, we quantified synapse number at the presynaptic NMJ on muscle DA1, measured by
123 active zones (visualized with the nc82 antibody against the active zone protein Bruchpilot (Wagh et
124 al., 2006)). This describes a more complex relationship. As previously published, a moderate increase
125 in activity, e.g., rearing larvae at 29°C, causes both more boutons and also more active zones to be
126 formed, potentiating transmission at the NMJ (Sigrist et al., 2003). In contrast, further increases in
127 network activity, as effected by rearing larvae at 32°C or by cell-specific dTrpA1-mediated
128 motoneuron activation at increasing temperatures led to progressive active zone reductions (Figure
129 1D, E).
130 We then looked at activity-regulated structural changes of the postsynaptic dendritic arbor
131 of the aCC motoneuron, which is known to be plastic during embryonic and larval stages (Hartwig et
132 al., 2008; Tripodi et al., 2008). To this end, we targeted GAL4 and dTrpA1 expression to individual
133 aCC motoneurons (Ou et al., 2008). Morphometric analysis revealed that the size of the aCC
134 postsynaptic dendritic arbor decreased with rising levels of temperature-gated dTrpA1 activity
135 (Figure 1F, G). We and others previously showed that dendritic length of these neurons correlates
136 with input synapse number and synaptic drive (Schneider-Mizell et al., 2016; Zwart et al., 2013).
137 In summary, we find that the synaptic terminals of larval motoneurons undergo titratable
138 structural changes in response to neuronal overactivation. Postsynaptic dendritic arbor size, and by
139 inference synapse number and synaptic drive (Zwart et al., 2013), negatively correlate with
140 activation levels. At the presynaptic NMJ, synapse number also correlates negatively with activation
141 level - bar a narrow low level activity window that can lead to potentiation (Ataman et al., 2008;
142 Piccioli and Littleton, 2014; Sigrist et al., 2003). Boutons provide an additional anatomical readout
143 for NMJ plasticity, increasing in number with levels of activity. However, no functional significance of
144 bouton number and size has been documented and changes in these bouton parameters are not
145 predictive of changes in synaptic transmission (Campbell and Ganetzky, 2012).
146

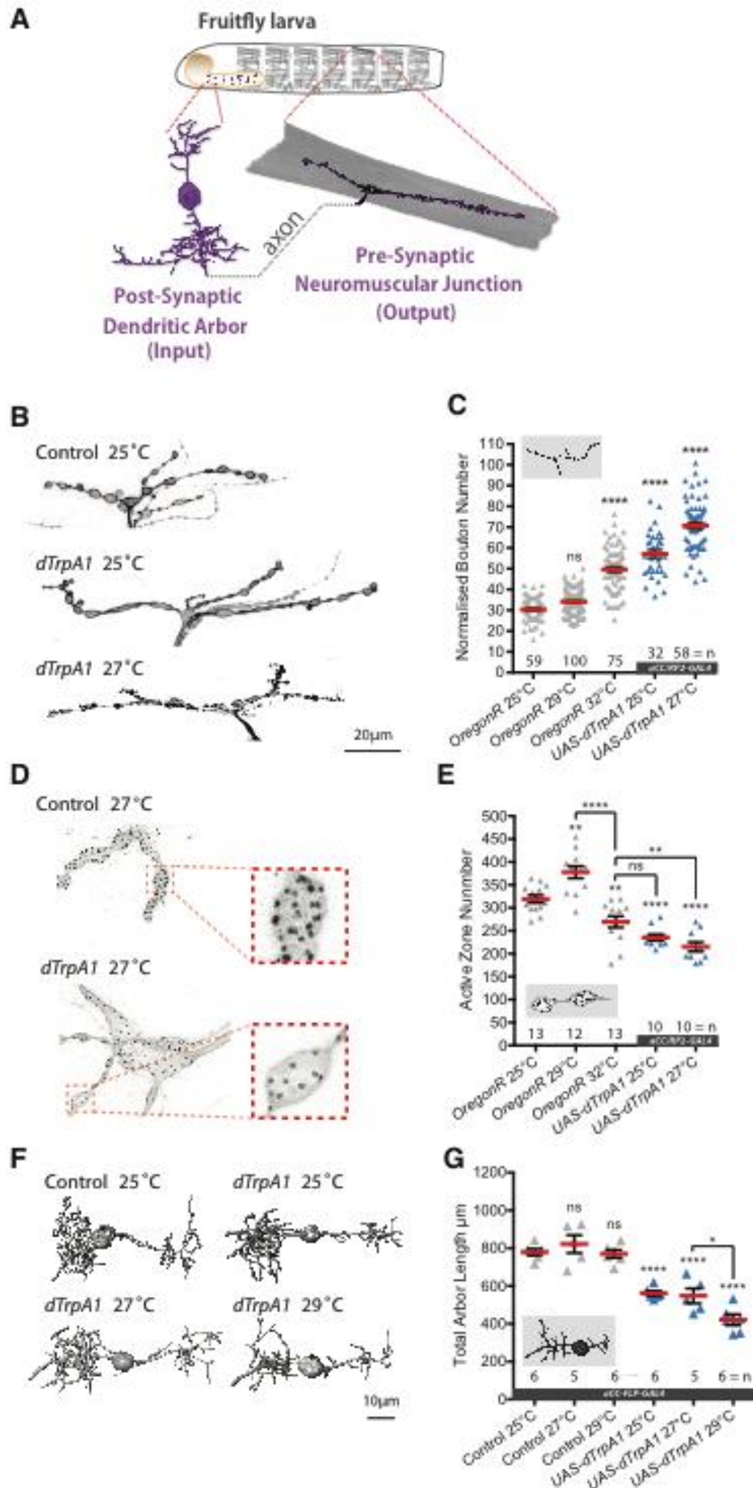

147

148 ***Figure 1: Adaptive structural synaptic plasticity at motoneuron input and output terminals in***
149 ***response to increased neuronal activity.*** *(**A**) Graphical illustration of a stereotypical larval*
150 *motoneuron (MN) (adapted from Kohsaka et al. (2012)). Pre-motor interneurons make synaptic*
151 *connections with the MN dendritic arbor (input) in the larval ventral nerve cord (equivalent of*
152 *mammalian spinal cord). The MN extends an axonal projection into the periphery where it connects*
153 *with a target muscle via an NMJ, characterized by varicose swellings (boutons) each containing*
154 *multiple individual neurotransmitter release sites (active zones). (**B** and **C**) Representative images of*

155 *muscle DA1 [muscle 1 according to (Crossley, 1978)] NMJs from 3rd instar larvae (100hrs ALH). Dot-*
156 *plot quantification shows NMJ bouton number increases in response to systemic and cell-specific*
157 *activity increases. (**D** and **E**) Active zone number increases following low-level overactivation (29°C),*
158 *but progressively reduces upon stronger overactivation. (**F** and **G**) Digital reconstructions and dot*
159 *plots show that overactivation leads to reduced total dendritic arbor length of aCC motoneurons*
160 *(24hrs ALH). 'aCC/RP2-GAL4' expresses GAL4 in all, 'aCC-FLP-GAL4' in single aCC and RP2*
161 *motoneurons (see Online Methods for details); 'Control' in (B-G) is heterozygous aCC/RP2-GAL4 or*
162 *aCC-FLP-GAL4, achieved by crossing the respective GAL4 line to Oregon-R wild type. Mean +/- SEM,*
163 *ANOVA, ns = not significant, *P<0.05, **P<0.01, ***P<0.001, ****P<0.0001, n = replicate number.*
164 *Comparisons with control are directly above data points.*
165
166
167 **Neuronal overactivation leads to ROS generation in presynaptic terminals.**
168 Next, we asked if *in vivo* overactivation of individual motoneurons is associated with increased ROS
169 levels, as reported for hippocampal neurons in culture (Hongpaisan et al., 2004). To this end, we co-
170 expressed in aCC and RP2 motoneurons the mitochondrion-targeted ratiometric ROS reporter *UAS-*
171 *mito-roGFP2-Orp1* (Gutscher et al., 2009) along with *UAS-dTrpA1*. We focused on mitochondria at
172 the muscle DA1 NMJs of wandering third instar larvae (100 hrs ALH). Quantification shows a clear
173 trend of increasing temperature and dTrpA1-mediated activation resulting in progressively greater
174 mean oxidation levels of this ROS sensor in mitochondria at the NMJ (Figure 2A). These data show
175 that *in vivo* dTrpA1-mediated overactivation of *Drosophila* larval motoneurons leads to increased
176 mitochdondrial ROS at presynaptic NMJs.
177
178
179 **Activity generated ROS regulate structural plasticity at synaptic terminals**
180 We then tested whether or not ROS are required for activity-dependent structural synaptic terminal
181 plasticity. To this end we increased neuronal activity in the aCC and RP2 motoneurons via dTrpA1
182 expression, rearing larvae at 25°C, the lower threshold of dTrpA1 activation that leads to activity-
183 dependent changes of synaptic terminals. At the same time we additionally over-expressed in these
184 neurons ROS scavenging enzymes: Superoxide Dismutase 2 (SOD2), which catalyses O_2^- to H_2O_2
185 reduction; or Catalase, which converts H_2O_2 into H_2O and O_2. Over-expression of either ROS
186 scavenger enzyme alone showed no effect on NMJ bouton number (Figure 2B). For Catalase over-
187 expression we further quantified active zone number at the NMJ and dendritic arbor size and there
188 too found this indistinguishable from controls (Figure 2C, 3B). In contrast, co-expression of *UAS-*
189 *Catalase* with *UAS-dTrpA1* significantly counteracted changes in bouton and active zone number
190 otherwise caused by dTrpA1-mediated neuronal overactivation (25°C) (Figure 2B, 3B). Similarly, at
191 the motoneuron input terminals in the CNS, Catalase co-expression rescued dendritic arbor size
192 (Figure 2C). Conversely, SOD2 co-expression enhanced the dTrpA1-mediated increase of bouton
193 number at the NMJ, presumably by potentiating conversion of activity-generated increase of O_2^- into
194 H_2O_2 (Figure 2B). We next asked if increasing neuronal ROS was sufficient to invoke structural
195 plasticity in the absence of dTrpA1 activity manipulations. Indeed, cell-specific RNAi knock down of
196 any one of three endogenous ROS scavengers, SOD1, SOD2 or Catalase, led to NMJs with increased
197 bouton number, in agreement with a prior study by Milton et al. (2011), who had demonstrated

198 oxidative stress causing NMJ growth. These structural NMJ changes are similar to those produced by
199 neuronal overactivation (Figure 2B) and implicate ROS, specifically H_2O_2, as a signal for regulating
200 activity-dependent structural plasticity at input and output terminals.

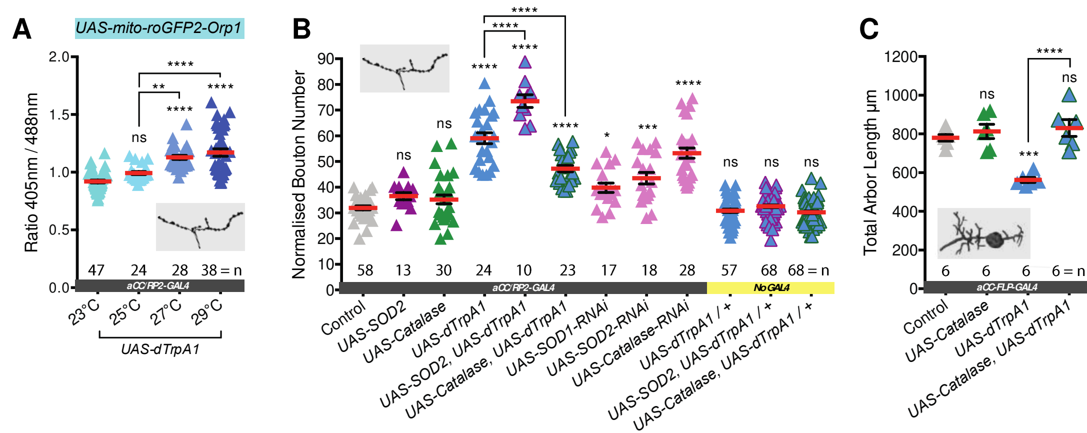

201

202

203 ***Figure 2: Neuronal activation leads to generation of synaptic ROS that regulate structural***
204 ***plasticity at input and output terminals.*** *(**A**) Elevated cell-specific activity increases mitochondrial*
205 *ROS production at NMJs. Dot plots of mitochondrion-targeted ratiometric H_2O_2 sensor (UAS-mito-*
206 *roGFP2-Orp1 (Gutscher et al., 2009)) in wandering 3rd instar larval NMJs (100hrs ALH) at 23˚C*
207 *(control, dTrpA1 inactive), 25˚C (moderate), 27˚C (strong) and 29˚C (very strong) dTrpA1-mediated*
208 *overactivation. (**B**) Bouton number at the NMJ is increased by UAS-dTrpA1-mediated overactivation.*
209 *This is exacerbated by co-expression of UAS-SOD2 (converts O_2^- to H_2O_2) and rescued by expression of*
210 *the H_2O_2 scavenger UAS-Catalase. Cell-specific ROS elevation by scavenger knockdown is sufficient to*
211 *induce NMJ elaboration. aCC/RP2-GAL4, 'Control' is aCC/RP2-GAL4 alone. (**C**) Total dendritic arbor*
212 *length is reduced by single cell overactivation, but rescued by co-expression of the H_2O_2 scavenger*
213 *UAS-Catalase (aCC motoneurons, 24hr ALH). aCC-FLP-GAL4, 'Control' is aCC-FLP-GAL4 alone,*
214 *heterozygous, achieved by crossing the GAL4 driver to Oregon-R wild type flies. Larvae were reared*
215 *at 25°C unless indicated otherwise. Mean +/- SEM, ANOVA, ns = not significant, *P<0.05, **P<0.01,*
216 *****P<0.001, ****P<0.0001, n = replicate number.*

217

218

219 **DJ-1ß acts as a ROS sensor in neurons**

220 We then investigated how neurons might sense changes in activity-induced ROS levels. ROS are
221 known to post-translationally modify many different proteins, principally on cysteine or methionine
222 residues, including transcription factors, cytoskeletal proteins, cell adhesion molecules and
223 phosphatases (for review see (Milton and Sweeney, 2012)). We identified DJ-1ß, the fly ortholog of
224 DJ-1 (PARK7), as a candidate ROS sensor. *DJ-1* codes for a highly conserved, ubiquitously expressed
225 redox-sensitive protein, that protects against oxidative stress and regulates mitochondrial function
226 (Ariga et al., 2013; Nagakubo et al., 1997). A mutant allele is also linked to a rare form of familial
227 Parkinsonism (Bonifati et al., 2003). *DJ-1* null mutants are viable without any conspicuous defects
228 and adult flies have been reported to have increased sensitivity to oxidative stress, e.g., as induced
229 by exposure to paraquat or H_2O_2 (Meulener et al., 2005). We found that *DJ-1ß* null mutant (*DJ-1ß*$^{\Delta 93}$)
230 larvae develop normally, indistinguishable from wild type controls, and have structurally normal

231 NMJs (Figure 3A and Figure 3-supplement 1). Interestingly, in larvae homozygous for the *DJ-1ß*^{Δ93}
232 null mutation, NMJs fail to respond to elevated ROS levels and do not generate additional boutons,
233 as typical for controls when feeding 10mM paraquat, which causes elevated O_2^- release from
234 mitochondrial complex 1, or 10mM Diethyl maleate (DEM), which inactivates the ROS scavenger
235 glutathione (Milton et al., 2011) (Figure 3A). Similarly, loss of DJ-1ß also significantly rescues NMJ
236 bouton addition phenotypes induced by targeted expression of the ROS generator Duox in aCC and
237 RP2 motoneurons, or their dTrpA1-mediated overactivation (Figure 3A). *DJ-1ß*^{Δ93} mutant larvae also
238 failed to produce the presynaptic bouton and active zone addition that result from raising larvae at
239 29°C (Sigrist et al., 2003) (Figure 3 – supplement 2). The neuronal requirement for *DJ-1ß* was further
240 tested via rescue experiments where neuronal *UAS-DJ-1ß* miss-expression in a *DJ-1ß* null-mutant
241 background proved sufficient to re-establish sensitivity to DEM (see Figure 3 – supplement 3). Next,
242 we cell-autonomously changed the ability of DJ-1ß to act as a redox sensor. DJ-1 is known to form
243 dimers (Lin et al., 2012a). We expressed in aCC and RP2 motoneurons a dominant-acting mutant
244 form of DJ-1ß that is non-oxidizable at the conserved cysteine 104, *UAS-DJ-1ß*^{C104A} (Meulener et al.,
245 2006). Expression of DJ-1ß^{C104A} abrogated ROS-induced (following DEM feeding) as well as dTrpA1
246 activity-mediated NMJ structural adjustment, both with respect to bouton number (Figure 3A) and
247 active zone number (Figure 3B). Looking at activity-dependent structural plasticity of the
248 postsynaptic dendritic arbor, we found this is sensitive to *DJ-1ß* levels; halving the copy number of
249 *DJ-1ß* (in *DJ-1ß*^{Δ93}*/+* heterozygotes) was sufficient to significantly suppress dTrpA1-mediated changes
250 to dendritic arbor size (Figure 3C).
251 In summary, these data show that DJ-1ß is necessary for activity-induced structural changes,
252 compatible with DJ-1ß functioning as a sensor for ROS. DJ-1ß appears to be required in motoneurons
253 for increasing NMJ bouton and active zone numbers in response to mild overactivation regimes that
254 lead to potentiation of transmission at the NMJ (raising larvae at 29°C) (Sigrist et al., 2003). At higher
255 levels, as induced by dTrpA1-mediated overactivation, DJ-1ß is also necessary in motoneurons,
256 though under these conditions for decreasing active zone numbers at the NMJ and the size of
257 postsynaptic dendritic arbors.
258

259

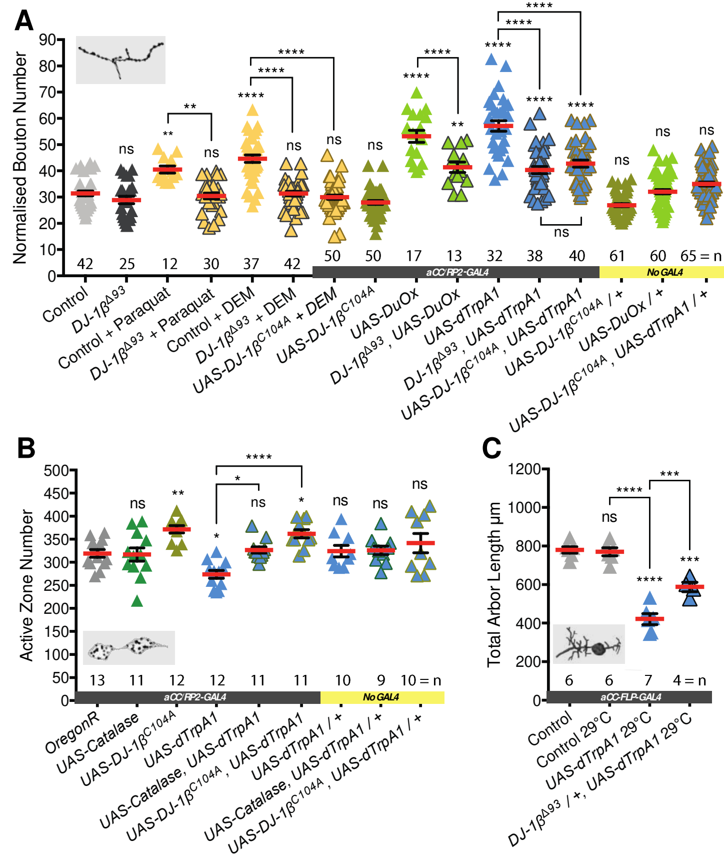

260 ***Figure 3: DJ-1ß senses ROS and regulates activity-induced neural plasticity.*** *(**A**) DJ-1ß is required for*
261 *ROS and neuronal-activity-induced NMJ elaboration (100hrs ALH). Larvae reared at 25°C. (**B**) Cell-*
262 *specific expression of DJ-1ß^{C104A}, non-oxidizable on conserved cysteine C104, prevents activity-*
263 *induced reduction of active zone number. 'Control' is aCC/RP2-GAL4 alone. Larvae were reared at*
264 *25°C. (**C**) Activity-generated ROS sensing is dose sensitive. Removal of one copy of DJ-1ß (in DJ-1ß^{Δ93} /*
265 *+ heterozygotes) is sufficient to significantly rescue activity-induced reduction of total dendritic arbor*
266 *length of motoneurons in 24hr ALH larvae. 'Control' is aCC-FLP-GAL4 alone, heterozygous, achieved*
267 *by crossing the GAL4 driver to Oregon-R wild type flies.*

268

269

270 PTEN and PI3K are downstream effectors of the DJ-1ß ROS sensor

271 Next, we looked for downstream effector pathways responsible for implementing activity and ROS-
272 dependent structural plasticity. DJ-1 is a known redox-regulated inhibitor of PTEN and as such
273 disinhibits PI3Kinase signaling (Kim et al., 2005; Kim et al., 2009b). PI3Kinase was previously shown
274 to regulate bouton and active zone number during NMJ development (Jordán-Álvarez et al., 2012;
275 Martín-Peña et al., 2006). To test if DJ-1ß - PTEN interactions mediate ROS-dependent NMJ
276 adjustments, we performed genetic interaction experiments in the context of DEM-induced ROS
277 elevation (Milton et al., 2011) (Figure 4A). We used different DEM dosages to generate a dose-
278 response curve and focused on changes in NMJ bouton number as a quantitative readout. We found
279 that in controls bouton number increases linearly with exposure to increasing DEM concentrations,
280 peaking at 15mM DEM (Figure 4A). Removal of one copy of *DJ-1ß* (*DJ-1ß^{Δ93}/+*) was sufficient to
281 suppress these DEM-induced increases in bouton number. Conversely, removing one copy of the

PI3Kinase antagonist PTEN (*PTEN*^{CO76}*/+*) resulted in increased sensitivity to DEM, as indicated by the left-shifted dose response curve. Larvae made heterozygous mutant for both *DJ-1ß* and *PTEN* (*PTEN*^{CO76}*/+; DJ-1ß*$^{\Delta 93}$*/+*) were overall less sensitive to DEM than controls, though at higher concentrations displayed greater sensitivity to DEM than *DJ-1ß*$^{\Delta 93}$*/+* heterozygotes, as might be expected when lowering *PTEN* copy number. These genetic interactions support previous studies (Kim et al., 2005) and complement biochemical data that showed increased binding of DJ-1ß to PTEN following oxidation by H_2O_2, thus effecting PTEN inhibition (Kim et al., 2009b).

To further test specificity, we manipulated PTEN and PI3Kinase activities in single cells. Targeted knock-down of endogenous PTEN in aCC and RP2 motoneurons sensitized these to ROS, exacerbating the DEM-induced bouton addition phenotype (Figure 4B). In contrast, over-expression of PTEN or mis-expression of a dominant negative form of PI3Kinase significantly reduced NMJ elaboration normally caused by DEM exposure or dTrpA1-mediated overactivation (Figure 4B). Together these genetic interactions suggest a working model whereby PTEN and PI3Kinase act downstream of DJ-1ß; and neural activity-generated ROS, via oxidation of DJ-1ß, leads to PTEN inhibition. This in turn facilitates a rise in PI3Kinase / PIP_3 signaling, which mediates at least part of the structural synaptic terminal plasticity by regulating bouton and active zone number at the NMJ (Figure 7).

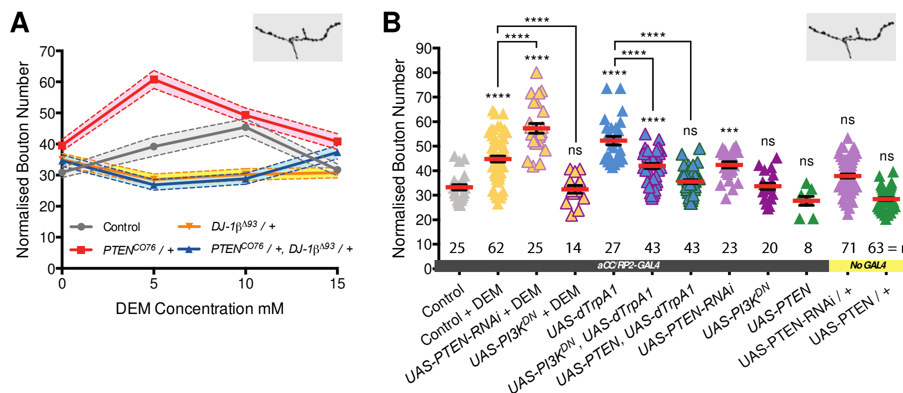

Figure 4: DJ-1β signals via PTEN and PI3Kinase to regulate ROS and activity-induced NMJ elaboration. *(**A**) DJ-1β and PTEN genetically interact to regulate systemic ROS-induced NMJ elaboration. NMJ bouton number varies with ROS (DEM) levels (grey data). Removal of one copy of PTEN sensitizes (red) while heterozygosity for DJ-1ß desensitizes NMJs to ROS levels (yellow), partially restored in double heterozygotes (blue). Dashed boundaries indicate 95 % confidence intervals (n≥38). (**B**) Systemic ROS and activity-induced NMJ structural adjustments require PTEN and PI3Kinase signaling. Over-expression of the PI3Kinase antagonist PTEN or a dominant negative PI3Kinase form abrogates activity-induced NMJ elaboration. 'Control' is aCC/RP2-GAL4 alone, heterozygous, achieved by crossing the GAL4 driver to Oregon-R wild type flies. Mean +/- SEM, ANOVA, ns = not significant, **P<0.01, ***P<0.001, ****P<0.0001, n = replicate number.*

Activity-regulated ROS signaling is necessary for homeostatic adjustment of synaptic transmission at the NMJ

To complement our studies of structural plasticity at the NMJ, we carried out sharp electrode recordings from the target muscle co-innervated by the aCC and RP2 motoneurons, muscle dorsal

316 acute 1 (DA1) (Hoang and Chiba, 2001; Landgraf et al., 2003; Mauss et al., 2009). In Oregon-R wild
317 type larvae we recorded evoked excitatory junction potentials (eEJPs) of 18 ±2mV (Figure 5A, D) and
318 miniature excitatory junction potentials (mEJPs) indicative of spontaneous vesicle fusion of 1mV
319 (Figure 5B, D). Therefore, on average each action potential triggers fusion of 18 vesicles at this NMJ
320 (quantal content) (Figure 5C).

321 We investigated how these parameters of NMJ transmission might change following cell-
322 specific dTrpA1-mediated overactivation of the aCC and RP2 motoneurons (at 25°C and 27°C). We
323 then tested if these activity-driven changes in transmission required ROS signaling, by co-expressing
324 the ROS scavenger Catalase or by abrogating ROS sensor function through co-expression of the
325 dominant acting, non-oxidizable DJ-1ß variant, DJ-1ß^{C104A}. Transmission at NMJs in *Drosophila* is
326 characteristically robust due to several homeostatic regulatory mechanisms working toward
327 maintaining constancy of eEJPs (for reviews see (Frank, 2014; Frank et al., 2013; Harris and Littleton,
328 2015)). Following dTrpA1-mediated overactivation (rearing larvae at 25°C and 27°C) evoked NMJ
329 transmission at the muscle DA1 NMJ remains intact and homeostatically balanced (Figure 5A, D).
330 Recordings from controls and larvae with dTrpA1 expressing motoneurons reared at 27°C showed
331 noticeably less variability of eEJP amplitude than those made from genetically identical siblings
332 reared at 25°C, the dTrpA1 activation threshold, potentially reflecting variable efficacy in
333 motoneuron manipulation (Hamada et al., 2008; Pulver et al., 2009). Overexpression of either
334 Catalase or DJ-1ß^{C104A} has no effect on eEJP amplitude. However, co-expression of Catalase with
335 dTrpA1-mediated overactivation leads to reduction of eEJP amplitude to 7-9mV. This suggests that
336 ROS are required for mechanisms that homeostatically maintain eEJP amplitude (Figure 5A, D).

337 In contrast, the amplitude of spontaneous vesicle fusion events (mEJP) adjusts inversely with
338 progressively stronger overactivation of motoneurons. These reductions in mEJP amplitude are not
339 specific to dTrpA1-mediated overactivation. Along with others (Ueda and Wu, 2015; Yeates et al.,
340 2017) we also recorded similarly reduced mEJP amplitudes in wild type Oregon-R larvae that had
341 been reared at an elevated temperature (27°C *versus* controls reared at 25°C) (Figure 5B). Co-
342 expression of DJ-1ß^{C104A} abrogates this activity-dependent reduction of mEJP amplitude (Figure 5B,
343 D), while Catalase co-expression has no effect on mEJP amplitude. Our analysis of quantal content
344 (the mean number of vesicles releasing transmitter per action potential, calculated as the ratio of
345 eEJP/mEJP amplitudes) showed that dTrpA1-mediated motoneuron over-activation at 27 ^{o}C leads to
346 significantly increased quantal content, and that this is brought back to control levels with co-
347 expression of the H_2O_2 scavenger Catalase, as might be expected from the reduced eEJP amplitudes
348 under such conditions.

349 In summary, evoked transmission at the NMJ is homeostatically maintained despite
350 increased dTrpA1-mediated neuronal overactivation. The maintenance of eEJP amplitude requires
351 ROS and is compromised when the H_2O_2 scavenger Catalase is expressed by the presynaptic
352 motoneuron. Activity-regulated changes in mEJP amplitude also depend on ROS signaling, though
353 this is not impacted by the over-expression of cytoplasmic Catalase; instead we found this aspect of
354 synaptic transmission sensitive to oxidation of DJ-1ß.
355

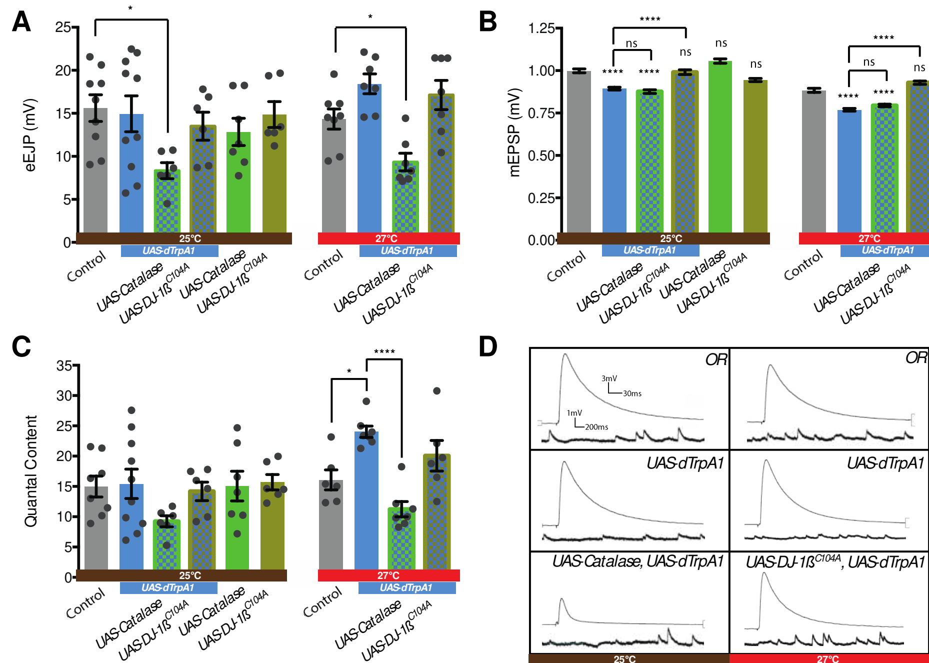

Figure 5: Pre-synaptic ROS regulate the maintenance of eEJP amplitude and DJ-1ß function is required for the reduction of mEJP amplitude during overactivation. *(A) Overactivated motoneurons (expressing dTrpA1 at 25°C, 27°C) show similar eEJP amplitude to control, despite reduced mEJP amplitude (see B). Catalase co-expression prevents this adaptation, significantly reducing eEJP amplitude, whereas DJ-1ß appears not to be required. (B) Increased neuronal activity, mediated by dTrpA1 expression at 25°C or by elevating ambient temperature to 27°C, reduces mEJP amplitude. Co-expression of DJ-1ß^{C104A} rescues this effect. (C) Quantal content (eEJP amplitude / mEJP amplitude) shows no significant difference between groups due to high variance within some conditions. (D) Representative eEJP and mEJP traces. ANOVA, ns = not significant, * P<0.05, **** P<0.0001.*

Structural plasticity of synaptic terminals is required for homeostatic adjustment of locomotor behavior

We wondered what impact the observed activity-ROS-regulated structural adjustments might have on network output. To test this we used larval crawling speed as a quantifiable readout for a simple locomotor behavior. In agreement with a previous study (Sigrist et al., 2003; Zhong and Wu, 2004), we found that crawling speed increases upon acutely shifting mid-3rd instar larvae (72 hours ALH) to higher ambient temperatures (e.g., from 25°C to 29°C or 32°C) (blue data in Figure 6A). This is to be expected given that these animals have an innate preference for approximately 25°C (Dillon et al., 2009; Hamada et al., 2008; Luo et al., 2016; Rosenzweig et al., 2005). In contrast, following prolonged exposure to an elevated temperature, achieved by rearing larvae at 29°C or 32°C, larvae crawled at the same speed characteristic of controls reared at 25°C (average of 0.65 – 0.72mm/second; grey horizontal dotted line in Figure 6A). This crawling speed adaptation is suggestive of a homeostatic adjustment of the locomotor network. Increased network drive might be counteracted by reduced neuronal excitability and/or synaptic input, thus allowing motor output

383 to be returned to the default crawling speed; in which case one would expect greater adjustment in
384 larvae reared at 32°C than 29°C. To reveal such adjustments we acutely shifted warmth-adapted
385 animals to 25°C, which caused reduced crawling speed (green data in Figure 6A). Indeed, following
386 this downward-shift 32°C-adjusted larvae crawled significantly slower than 29°C-adjusted animals,
387 suggesting the degree of neuronal adjustment is proportional to the level of temperature-induced
388 overactivation. These experiments suggest that during prolonged activity manipulations the larval
389 locomotor network output homeostatically adjusts toward a default crawling speed.
390 Next, we wanted to test the role of the motoneurons in this form of network adjustment.
391 The motoneurons integrate all pre-motor input within their dendritic arbors and produce the output
392 of the motor network. We targeted expression of dTrpA1 to the motoneurons (and other
393 glutamatergic cells, using *DvGlut-T2A-GAL4*) and reared these animals at 27°C, a temperature that
394 robustly activates dTrpA1-expressing neurons (Hamada et al., 2008; Pulver et al., 2009). Upon acute
395 removal of this overstimulation (by shifting animals to 22°C where the dTrpA1 channel is closed)
396 larval crawling speed reduced significantly relative to non-dTrpA1 expressing controls (Figure 6B).
397 We then asked whether this ROS-mediated structural plasticity of synaptic terminal growth was
398 required for homeostatic adjustment of larval crawling speed, which ensues after prolonged
399 overactivation. We manipulated the ability of neurons to sense increases in ROS levels by targeting
400 expression of the dominant acting non-oxidizable DJ-1ß^{C104A} variant to motoneurons. We then tested
401 the behavior of these animals for adjustment in response to chronic temperature-induced elevation
402 of motor network activity. Our previous set of experiments showed that expression of non-
403 oxidizable DJ-1ß^{C104A} in motoneurons prevents structural adjustment of bouton number and the
404 decrease in active zone number normally caused by overactivation (see Figures 3A & 3B). Expression
405 of non-oxidizable DJ-1ß^{C104A} in motoneurons *per se* did not alter larval crawling speed at the control
406 temperature of 25°C. However, when rearing these larvae at 32°C, which is associated with elevated
407 motor network activation, unlike controls they failed to homeostatically adjust toward the default
408 crawling speed (Figure 6C). Consequently, such larvae reared at elevated temperatures (29°C or
409 32°C) also responded less strongly than controls to acute temperature downshifts (Figure 6C). These
410 data suggest that activity-induced structural plasticity, implemented through the ROS sensor DJ-1ß,
411 is necessary for activity-directed homeostatic adjustment of larval locomotor behavior.
412

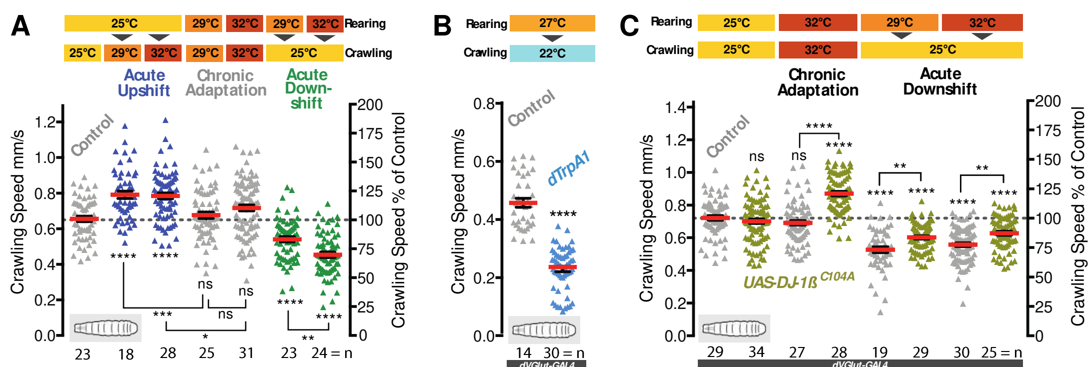

413
414
415 ***Figure 6: Adaptive behavioral plasticity in response to chromic locomotor overactivation. (A)***
416 *Larval motor network activity, assayed by crawling speed 72hrs after larval hatching (AHL), increases*

417 *in response to acute temperature upshifts (blue) in wild type larvae. In contrast, with prolonged*
418 *exposure (grey) to elevated temperatures (29°C or 32°C) the motor network adapts homeostatically*
419 *generating the same crawling speed as 25°C reared controls. This adaptation is further revealed by*
420 *acute temperature downshifts (green). Each data point represents crawling speed from an individual*
421 *uninterrupted continuous forward crawl, n = specimen replicate number, up to 3 crawls assayed for*
422 *each larva. Genotype = OregonR. (**B**) Prolonged overactivation targeted to motoneurons (dVGlut-*
423 *GAL4; UAS-dTrpA1) also leads to adaptation with reduced crawling speed (dTRPA1 channels open at*
424 *27°C, closed at 22°C). Mean +/- SEM, control is dVGlut-GAL4 / +. ****P<0.0001 students t test, n =*
425 *replicate number. (C) Larvae with expression of UAS-DJ-1β^{C104A} targeted to motoneurons (dVGlut-*
426 *GAL4) are unable to adapt motor network output (crawling speed) to elevated rearing temperatures.*
427 *Control is dVGlut-GAL4 alone, in heterozygous condition. Each data point represents crawling speed*
428 *from an individual uninterrupted continuous forward crawl, n = specimen replicate number, up to 3*
429 *crawls assayed for each larva. Mean +/- SEM, ANOVA, ns = not significant, *P<0.05, **P<0.01,*
430 ****P<0.001, ****P<0.0001.*
431

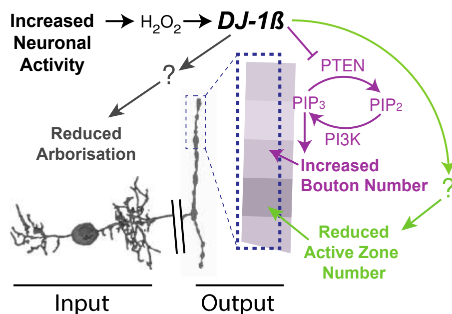

432
433
434 **Figure 7: Model summary**. *DJ-1β* is a redox signaling hub that coordinates structural synaptic
435 plasticity at motoneuron synaptic input and output terminals. Activity-induced ROS oxidize *DJ-1β*,
436 leading to PTEN inhibition and thus to a gain in PI3Kinase signaling, which regulates activity-induced
437 NMJ elaboration of boutons and active zones. At higher activity/ROS thresholds additional, yet to be
438 defined, pathways downstream of *DJ-1β* are activated, implementing adaptive reductions of active
439 zones at the NMJ and dendritic arbor length in the CNS.
440
441

442 Discussion

443

444 ROS signaling is required for neuronal activity-dependent structural plasticity

445 Building on previous work that had shown oxidative stress as inducing NMJ growth (Milton et al.,
446 2011), we have in this study identified ROS as obligatory signals for activity-regulated structural
447 plasticity. We further show that ROS are also sufficient to bring about structural changes at synaptic
448 terminals that largely mimic those induced by neuronal overactivation (Figure 2B, C). A
449 mitochondrially targeted ROS reporter (Albrecht et al., 2011; Gutscher et al., 2009) suggests a
450 positive correlation between levels of neuronal activity and ROS generated in mitochondria,
451 potentially as a byproduct of increased ATP metabolism or triggered by mitochondrial calcium influx

452 (Peng and Jou, 2010) (Figure 2A). Although we did not specifically investigate the nature of the
453 active ROS in this context, three lines of evidence suggest that H_2O_2, generated by the dismutation of
454 O_2^-, is the principal signaling species. First, under conditions of neuronal overactivation (but not
455 control levels of activity) over-expression of the O_2^- to H_2O_2 converting enzyme SOD2 potentiated
456 structural plasticity phenotypes (Figure 2B). Second, over-expression of the H_2O_2 scavenger Catalase
457 efficiently counter-acts all activity-induced changes we have quantified, at both postsynaptic
458 dendritic and presynaptic NMJ terminals. Third, over-expression of the H_2O_2 generator Duox in
459 motoneurons is sufficient to induce NMJ bouton phenotypes that mimic overactivation (Figure 3A).
460 In addition to mitochondria, other sources of ROS include several oxidases, notably NADPH oxidases.
461 These have been implicated during nervous system development in the regulation of axon growth
462 and synaptic plasticity (Kishida et al., 2006; Munnamalai and Suter, 2009; Munnamalai et al., 2014;
463 Olguín-Albuerne and Morán, 2015; Serrano et al., 2003; Tejada-Simon et al., 2005; Wilson et al.,
464 2016; Wilson et al., 2015). NADPH oxidases can be regulated by NMDA receptor stimulation
465 (Brennan et al., 2009) and activity-associated pathways, including calcium, Protein kinases C and A
466 and calcium/calmodulin-dependent kinase II (CamKII) (Bánfi et al., 2004; Massaad and Klann, 2011;
467 Pandey et al., 2011; Sorce et al., 2017; Tirone and Cox, 2007). The precise sources of activity-
468 regulated ROS, potentially for distinct roles in plasticity, will be interesting to investigate.
469

470 **ROS as gatekeepers of activity-dependent synaptic structural plasticity**

471 We demonstrated that ROS are necessary for activity-dependent structural plasticity of *Drosophila*
472 motoneurons, at both their postsynaptic dendrites in the CNS and presynaptic NMJs in the
473 periphery. The mechanisms by which ROS intersect with other known plasticity pathways now need
474 to be investigated. Among well documented signaling pathways regulating synaptic plasticity, are
475 Wnts (Budnik and Salinas, 2011), BMPs (Bayat et al., 2011; Berke et al., 2013), PKA, CREB and the
476 immediate early gene transcription factor AP-1 (Cho et al., 2015; Davis, 2006; Davis and Müller,
477 2015; Davis et al., 1998; Davis et al., 1996; Kim et al., 2009a; Koles and Budnik, 2012; Osses and
478 Henriquez, 2014; Sanyal et al., 2003; Sanyal et al., 2002; Sulkowski et al., 2014; Walker et al., 2013).
479 ROS signaling could be synergistic with other neuronal plasticity pathways, potentially integrating
480 metabolic feedback. Indeed, ROS modulate BMP signaling in cultured sympathetic neurons
481 (Chandrasekaran et al., 2015) and Wnt pathways in non-neuronal cells (Funato et al., 2006; Love et
482 al., 2013; Rharass et al., 2014). Biochemically, ROS are well known regulators of kinase pathways via
483 oxidation-mediated inhibition of phosphatases (Finkel and Holbrook, 2000; Tonks, 2006). Redox
484 modifications also regulate the activity of the immediate early genes Jun and Fos, which are required
485 for LTP in vertebrates, and in *Drosophila* for activity-dependent plasticity of motoneurons, both at
486 the NMJ and central dendrites (Hartwig et al., 2008; Jindra et al., 2004; Loebrich and Nedivi, 2009;
487 Milton and Sweeney, 2012; Milton et al., 2011; Sanyal et al., 2002). We therefore hypothesize that
488 ROS may provide neuronal activity-regulated modulation of multiple canonical synaptic plasticity
489 pathways.
490

491 **Structural plasticity and its coordination between pre- and postsynaptic terminals**

492 We focused on three aspects of synaptic terminal plasticity: dendritic arbor size in the CNS, and
493 bouton and active zone numbers at the NMJ. We used these as phenotypic indicators for activity-
494 regulated changes. By working with identified motoneurons we could observe adaptations across

the entire neuron, relating adjustments of postsynaptic dendritic input terminals in the CNS to changes of the presynaptic output terminals at the NMJ in the periphery. For the aCC motoneuron, the degree of neuronal overactivation correlates with changes in synaptic terminal growth: notably reductions of dendritic arbor size centrally and of active zones at the NMJ. Interestingly, presynaptic active zone numbers did not show a linear response profile. Within a certain range low-level activity increases lead to more active zones, associated with potentiation (as previously shown (Sigrist et al., 2003)); however, with stronger overactivation active zone number decrease (Figure 1D, E). Reduction of active zones, as we observed at the NMJ, and of Brp levels by increased activation was previously also reported in photoreceptor terminals of the *Drosophila* adult visual system (Sugie et al., 2015). At a finer level of resolution it will be interesting to determine how these activity-ROS-mediated structural changes might change active zone cytomatrix composition, which can impact on transmission properties, such as vesicle release probability (Davydova et al., 2014; Lazarevic et al., 2011; Matz et al., 2010; Peled et al., 2014; Weyhersmüller et al., 2011)

We previously found that in these motoneurons dendritic length correlates with the number of input synapses and with synaptic drive (Zwart et al., 2013). Therefore, we tentatively interpret the negative correlation between the degree of overactivation and the reduction in central dendritic arbors as compensatory. In agreement, we found that blockade of activity-induced structural adjustment targeted to the motoneurons prevents behavioral adaptation normally seen after prolonged overactivation (Figure 6). Less clear is if and how overactivation-induced structural changes at the NMJ might be adaptive. Unlike many central synapses that facilitate graded analogue computation, the NMJ is a highly specialized synapse with a large safety factor and intricate mechanisms that ensure constancy of evoked transmission in essentially digital format (Frank et al., 2013; Marrus and DiAntonio, 2005). Rearing larvae at 29°C (which acutely increases motor activity) leads to more active zones at the NMJ and potentiated transmission, yet these larvae crawl at the same default speed as other larvae reared at 25°C (control) or 32°C with reduced numbers of active zones (compare Figure 1E with Figure 6B). This suggests that at least with regard to regulating crawling speed, plasticity mechanisms probably operate at the network level, rather than transmission properties of the NMJ. Indeed, our recordings of transmission at the NMJ, and those reported by others, show homeostatic maintenance of eEJP amplitude irrespective of changes in bouton and active zone number (Figure 5) (Campbell and Ganetzky, 2012). Though in this study we focused on anatomical changes, we expect these structural adjustments to be linked to, and probably preceded by compensatory changes in neuronal excitability that have been documented (Baines et al., 2001; Davis, 2006; Davis et al., 1996; Davis et al., 1998; Driscoll et al., 2013; Frank et al., 2006; Frank et al., 2009; Gaviño et al., 2015; Giachello and Baines, 2016; Lin et al., 2012b; Mee et al., 2004; Müller and Davis, 2012; Wang et al., 2014; Younger et al., 2013; O'Leary et al., 2013; Prinz, 2006; Prinz et al., 2004).

Our observations of activity-regulated adjustments of both dendritic arbor size and NMJ structure give the impression of processes coordinated across the entire neuron. If this was the case, it could be mediated by transcriptional changes, potentially via immediate early genes (AP-1), which are involved in activity and ROS-induced structural changes at the NMJ (Milton et al., 2011; Sanyal et al., 2002) and motoneuron dendrites (Hartwig et al., 2008).

538 **Identification of DJ-1ß as a neuronal ROS sensor**

539 We discovered that in neurons the highly conserved protein DJ-1ß is critical for both
540 structural and physiological changes in response to activity-generated ROS (Figure 3 and Figure 5). In
541 neurons DJ-1ß might act as a redox sensor for activity-generated ROS. In agreement with this idea,
542 DJ-1ß has been shown to be oxidized by H_2O_2 at the conserved cysteine residue C106 (C104 in
543 *Drosophila*) (Lin et al., 2012a; Meulener et al., 2006). Oxidation of DJ-1 leads to changes in DJ-1
544 function, including translocation from the cytoplasm to the mitochondrial matrix, aiding protection
545 against oxidative damage (Blackinton et al., 2009; Canet-Avilés and Wilson, 2004; Waak et al., 2009)
546 and maintenance of ATP levels (Calì et al., 2015). We found that the ability of motoneurons to
547 respond to increased activation is potently sensitive to DJ-1ß dosage. It is also blocked by expression
548 of mutant DJ-1ß^{C104A} that is non-oxidisable on the conserved Cys104 (Hao et al., 2010; Meulener et
549 al., 2006). These observations suggest that DJ-1ß is critical to ROS sensing in neurons. They also
550 predict that cell type-specific DJ-1ß levels, and associated DJ-1ß reducing mechanisms, could
551 contribute to setting cell type-specific sensitivity thresholds to neuronal activity.

552

553

554

555

556 **DJ-1ß downstream pathways implement activity-regulated plasticity**

557 Our data suggest that DJ-1ß could potentially be part of a signaling hub. At the NMJ, this might
558 mediate plasticity across a range, from the addition of active zones associated with potentiation to,
559 following stronger overactivation, the reduction of active zones. We identified disinhibition of
560 PI3Kinase signaling as one DJ-1ß downstream pathway (Figure 4) (Kim et al., 2005; Kim et al., 2009b),
561 a well-studied intermediate in metabolic pathways and a known regulator of synaptic terminal
562 growth, including active zone addition (Jordán-Álvarez et al., 2012; Martín-Peña et al., 2006).
563 However, with stronger overactivation DJ-1ß might engage additional downstream effectors that
564 reduce active zone addition or maintenance, potentially promoting active zone disassembly. While
565 at the presynaptic NMJ PI3Kinase disinhibition explains activity-regulated changes in bouton
566 addition, different DJ-1ß effectors likely operate in the somato-dendritic compartment, which
567 responds to overactivation with reduced growth and possibly pruning (Brierley et al., 2009). Thus,
568 sub-cellular compartmentalization of the activity-ROS-DJ-1ß signaling axis could produce distinct
569 plasticity responses in pre- *versus* postsynaptic terminals.

570

571

572 **Homeostatic maintenance of synaptic transmission requires presynaptic ROS signaling**

573 Previous studies demonstrated a requirement for ROS for LTP (Huddleston et al., 2008; Kamsler and
574 Segal, 2003a; Kamsler and Segal, 2003b; Klann, 1998; Knapp and Klann, 2002; Lee et al., 2010) and
575 found learning defects in animal models with reduced NADPH oxidase activity (Kishida et al., 2006),
576 suggesting that synaptic ROS signaling might be a conserved feature of communication in the
577 nervous system. Our sharp electrode recordings from muscle DA1 revealed three interesting
578 aspects. First, that changing ROS signaling in the presynaptic motoneuron under normal activity
579 conditions does not obviously impact on NMJ transmission. Second, quenching of presynaptic ROS
580 by expression of Catalase under overactivation conditions led to a significant decrease in eEJP

581 amplitude and concomitantly reduced quantal content (Figure 5A, C). This shows that upon chronic
582 neuronal overactivation ROS signaling is critically required in the presynaptic motoneuron for
583 maintaining eEJP amplitude by increasing vesicle release at the NMJ. This could be achieved by
584 increasing vesicle release probability, which would counteract the reduction in active zone number
585 following a period of neuronal overactivation. In this context it is interesting that components of the
586 presynaptic release machinery, including SNAP25, are thought to be directly modulated by ROS
587 (Giniatullin et al., 2006), while others, such as Complexin, might be indirectly affected, e.g., via ROS-
588 mediated inhibition of phosphatases leading disinhibition of kinase activity (Cho et al., 2015). Third,
589 we found that overactivation of motoneurons leads to reduced mEJP amplitude, also recently
590 reported by others (Yeates et al., 2017). Curiously, mEJP amplitude, unlike eEJP amplitude, is
591 regulated by DJ-1ß, but is not impacted on by artificially increased cytoplasmic levels of the H_2O_2
592 scavenger Catalase. How it is that under conditions of neuronal overactivation eEJP and mEJP
593 amplitudes are differentially sensitive to cytoplasmic Catalase *versus* DJ-1ß oxidation is unclear,
594 though it marks these two processes as distinct. One possibility is that cytoplasmic Catalase changes
595 the local redox status, which could directly affect the properties of the presynaptic active zone
596 cytomatrix. In contrast, mEJP amplitude regulation might be indirect and cell non-autonomous, via
597 modulation of glutamate receptors in the postsynaptic target muscle (Davis et al., 1998).
598 Furthermore, these ROS-regulated adjustments in synaptic transmission are at
599 Thus, several distinct ROS responsive pathways appear to operate at the NMJ. Structural
600 adjustments in terms of synaptic terminal growth and synapse number are mediated by mechanisms
601 sensitive to DJ-1ß oxidation, potentially regulated via local reducing systems, including Catalase. In
602 addition and distinct from these structural changes, at least in part, are the ROS-regulated
603 adjustments in synaptic transmission that show different ROS sensitivities, one maintaining quantal
604 content of evoked transmission while the other reduces mEJP amplitude when neuronal activity
605 goes up (Figure 5B). It is conceivable that spatially distinct sources of ROS, e.g. mitochondria *versus*
606 membrane localized NADPH oxidases, with different temporal dynamics could potentially mediate
607 such differences in ROS sensitivities at the NMJ.
608
609 **Homeostatic adjustment of larval crawling speed depends on redox modification of DJ-1ß**
610 Our experiments exploring the potential behavioral relevance of activity-regulated structural
611 plasticity demonstrated that network drive is regulated by ambient temperature. Acute elevation in
612 ambient temperature produces faster crawling, while acute temperature reductions have the
613 opposite effect. In contrast, with chronic temperature manipulations, larval crawling returns to its
614 default speed (approx. 0.65 – 0.72mm/sec) (Figure 6A). This adaptation to chronic manipulations
615 might overall be energetically more favorable. It also allows larvae to retain a dynamic range of
616 responses to relative changes in ambient temperature (i.e. speeding up or slowing down).
617 Where in the locomotor network these adjustments take place remains to be worked out. It
618 is reasonable to assume that proprioceptive sensory neurons, and potentially also central recurrent
619 connections, provide feedback information that facilitates homeostatic adjustment of network
620 output. Our manipulations of the glutamatergic motoneurons show these cells are clearly important.
621 For example, cell type-specific overactivation of the glutamatergic motoneurons (via dTrpA1) on the
622 one hand, and blockade of activity-induced structural adjustment (by mis-expression of non-
623 oxidizable DJ-1ß^{C104A}) on the other demonstrated that ROS-DJ-1ß-mediated processes that we

showed important for structural adjustment are also required for implementing homeostatic tuning of locomotor network output (Figure 6B, C). The capacity of motoneurons as important elements in shaping motor network output, might be explicable in that these neurons constitute the final integrators on which all pre-motor inputs converge (Fushiki et al., 2016; Itakura et al., 2015; Kohsaka et al., 2014; Schneider-Mizell et al., 2016; Zwart et al., 2016).

In conclusion, here we identified ROS in neurons as novel signals that are critical for activity-induced structural plasticity. ROS levels regulated by neuronal activity have the potential for operating as metabolic feedback signals. We further identified the conserved redox-sensitive protein DJ-1ß as important to neuronal ROS sensing, and the PTEN/PI3Kinase synaptic growth pathway as a downstream effector pathway for NMJ growth in response to neuronal overactivation. These findings suggest that in the nervous system ROS operate as feedback signals that inform cells about their activity levels. The observation that ROS are important signals for homeostatic processes explains why ROS buffering is comparatively low in neurons (Bell et al., 2015). This view also shines a new light on the potential impact of ROS dysregulation with age or under neurodegenerative conditions, potentially interfering with neuronal adaptive adjustments and thereby contributing to network malfunction and synapse loss.

Competing interests: The authors declare that no competing interests exist.

Acknowledgements:

We would like to thank Richard Ribchester for invaluable help with setting up a rig for NMJ sharp electrode recording. Nancy Bonini, Tobias Dick, Jörg Grosshans, Karen Hibbard, Fanis Missirlis, Barret Peiffer and Alex Whitworth for generous reagent donations, and Akinao Nose and Hiroshi Kohsaka for kindly helping with figure 1. We would also like to thank Jimena Berni, Alex Whitworth and members of the Landgraf lab for valuable comments on the manuscript. This work was supported by BBSRC research grants (BB/IO1179X/1, BB/M002934/1) to ML and (BB/I012273/1, BB/M002322/1) to STS.

Materials and Methods

Electrophysiology. Late wandering third instar larvae were fillet dissected in standard HL3 buffer (adapted from (Stewart et al., 1994), 70mM NaCl, 5mM KCl, 20mM $MgCl_2$, 10mM $NaHCO_3$, 115mM Sucrose, 5mM HEPES, 1.5mM CaCl, pH 7.25) ventral surface down with a lateral incision in order preserve both the ventral and dorsal midlines. Suction (GC150F-10 Harvard Apparatus) and sharp

667 (GC100F-10 Harvard Apparatus) electrodes were pulled using a P-97 pipette puller (Sutter
668 Instrument Company). Sharp electrode muscle impalement (DA1 muscle, at the dorsal midline) and
669 inter-segmental nerve suction (ventral midline) were performed using an Olympus BX50WI
670 compound microscope with 10X air (Olympus 10x/0.25) and 20X dipping (Olympus UMPlanFL
671 20x/0.5w) objective lenses. Recordings were made at 21°C in HL3 using an Axopatch-1D amplifier
672 (Axon Instruments), a 1322A DigiData (Axon Instruments), a DS2A-MkII Constant Voltage Isolated
673 Stimulator (Digitimer Ltd.) and pCLAMP 10.4 acquisition software (Molecular Devices). mEJP (2-
674 3minutes) and eEJP (3 rounds of 20 stimulations, 5V) recordings were made in current-clamp mode
675 from muscle cells with an input resistance above 8MOhm and a stable resting membrane potential
676 between -40mV and -70mV. Analysis of eEJPs was performed using Clampfit10.6 (Molecular
677 Devices) and mEJPs using Mini-Analysis6.0.7 (Synaptosoft).
678
679 **Fly Strains and Husbandry.** Wild-type and transgenic strains were maintained on standard yeast–
680 agar–cornmeal medium at 25 °C. The following fly strains were used: *OregonR* and *PTEN*^{CO76}
681 (Bloomington Stock Center, Indiana University), *UAS-dTrpA1* (Hamada et al., 2008), *UAS-SOD2*
682 (Missirlis et al., 2003), *UAS-Catalase* (Missirlis et al., 2001), *UAS-Duox* (Ha, 2005), *DJ-11ß*$^{\Delta 93}$
683 (Meulener et al., 2005), *UAS-DJ-1ß*^{C104A} (Meulener et al., 2006), UAS-RNAi lines targeting *SOD1*,
684 *SOD2*, *Catalase* and *PTEN* (KK collection, Vienna Drosophila Resource Centre) (Dietzl et al., 2007),
685 *UAS-PI3K*^{DN} (Leevers et al., 1996), *UAS-PTEN* (Gao et al., 2000). The following two GAL4 expression
686 lines were used to target GAL4 to the aCC and RP2 motoneurons: *aCC-FLP-GAL4* (*eveRN2-Flippase,*
687 *UAS-myr::mRFP1, UAS-Flp, tubulin84B-FRT-CD2-FRT-GAL4*) (Roy et al., 2007) expresses GAL4
688 stochastically in single aCC and RP2 motoneurons allowing the imaging of aCC neurons in isolation,
689 as required for dendritic arbor resolution and reconstruction. *aCC/RP2-GAL4* (*eveRN2-GAL4* (Fujioka
690 et al., 2003)*, UAS-myr-mRFP1, UAS-Flp, tubulin84B-FRT-CD2-FRT-GAL4; RRaGAL4, 20xUAS-*
691 *6XmCherry::HA* (Shearin et al., 2014)) was used for NMJ analysis as it expresses GAL4 in every aCC
692 and RP2 motoneuron. *eveRN2-GAL4* expression is restricted to the embryo and FLPase-gated
693 *tubulin84B-FRT-CD2-FRT-GAL4* maintains GAL4 expression at high levels during larval stages.
694
695 **Dissection and Immunocytochemistry**
696 **1st Instar Ventral Nerve Cord (VNC).** Flies were allowed to lay eggs on apple juice-based agar
697 medium for 24 hrs at 25°C. Embryos were dechorionated using bleach (3.5 minutes room
698 temperature) then incubated (25°C) in pre-warmed Sorensen's saline (pH 7.2, 0.075 M) whilst
699 adhered to a petri dish. Hatched larvae (floating) were recovered hourly and transferred to pre-
700 warmed apple-juice agar plates supplemented with yeast paste. Larvae were allowed to develop for
701 a further 24 hrs (24 hrs after larval hatching, ALH) at 25°C, 27°C or 29°C prior to dissection in
702 Sorensen's saline. A fine hypodermic needle (30 1/2 G; Microlance) was used as a scalpel to cut off
703 the anterior end of each larva, allowing gut, fat body, and trachea to be removed. The ventral nerve
704 chord and brain lobes, extruded with viscera upon decapitation, were dissected out and transferred
705 to a cover glass coated with poly-L-lysine (Sigma-Aldrich), positioned dorsal side up in Sorensen's
706 saline. A clean cover glass was placed on top of the preparation, with strips of double-sided sticky
707 tape as spacers positioned along the edges.
708

709 **Wandering 3rd Instar.** Flies were allowed to lay eggs on apple-juice agar based medium overnight at
710 25°C, larvae were then incubated at 25°C or 27°C until the late wandering 3rd instar stage. Larvae
711 were reared on yeast paste colored with Bromophenol Blue Sodium Salt (Sigma-Aldrich) to allow
712 visualization of gut-clearance, an indicator of the late wandering 3rd instar stage. For Di-ethylmaleate
713 (DEM) (Sigma-Aldrich) and paraquat (Sigma-Aldrich) feeding, yeast paste was made using a 5 mM –
714 15 mM aqueous solution. Larvae were 'fillet' dissected in Sorensen's saline and fixed for 15 minutes
715 at room temperature in 4% formaldehyde (in Sorenson's saline). Specimens were then washed and
716 stained in Sorensen's saline containing 0.3% Triton X-100 (Sigma-Aldrich) using the following primary
717 / secondary antibodies; Goat-anti-HRP Alexa Fluor 594 (1:400) (Jackson ImmunoResearch Cat. No.
718 123-585-021), Rabbit-anti-dsRED (1:1200) (ClonTech Cat. No. 632496), Donkey-anti-Rabbit CF568
719 (1:1200) (Biotium Cat. No. 20098) incubated overnight at 4°C or 2 hrs at room temperature.
720 Specimens were mounted in EverBrite mounting medium (Biotium).
721
722 **Image Acquisition and Analysis**
723 **1st Instar Ventral Nerve Cord (VNC).** Ventral nerve cords were pre-screened for fluorescently
724 labeled, isolated, aCC motoneurons using a Zeiss Axiophot compound epifluorescence microscope
725 and a Zeiss Plan-Neofluar 40x/0.75 N.A. objective lens. Suitable VNCs were imaged immediately with
726 a Yokagawa CSU-22 spinning disk confocal field scanner mounted on an Olympus BX51WI
727 microscope, using a 60×/1.2 N.A. Olympus water immersion objective. Images were acquired with a
728 voxel size of 0.2 × 0.2 × 0.3 µm using a QuantEM cooled EMCCD camera (Photometrics), operated via
729 MetaMorph software (Molecular Devices). Dendritic trees were digitally reconstructed using Amira
730 Resolve RT 4.1 (Visualization Sciences Group and Zuse Institute), supplemented with a 3D
731 reconstruction algorithm (Evers et al., 2005; Schmitt et al., 2004), and images were processed using
732 Amira and ImageJ (National Institutes of Health).
733
734 **Wandering 3rd Instar.** Dissected specimens were imaged using a Leica SP5 point-scanning confocal,
735 and a 63x/1.3 N.A. (Leica) glycerol immersion objective lens and LAS AF (Leica Application Suite
736 Advanced Fluorescence) software. Confocal images were processed using ImageJ and Photoshop
737 (Adobe). Bouton number of the NMJ on muscle DA1 [1] from segments A3-A5 was determined by
738 counting every distinct spherical varicosity along the NMJ branch. DA1 muscles were imaged using a
739 Zeiss Axiophot compound microscope and a Zeiss Plan-Neofluar 10x/0.3 N.A. objective lens. Muscle
740 surface area (MSA) was determined by multiplying muscle length by width using ImageJ. In order to
741 correct for subtle differences in animal size (typically 5-10%) bouton number normalization was
742 performed using the following calculation: (mean control MSA / mean experimental MSA) x test
743 bouton number = normalized experimental bouton number.
744
745 **Ratiometric ROS Reporter.** *aCC/RP2-Gal4* was used to drive the expression of *UAS-mito-roGFP2-*
746 *Orp1* (Albrecht et al., 2011; Gutscher et al., 2009) in all aCC and RP2 motoneurons. Wandering third
747 instar larvae were fillet dissected in PBS-NEM (137mM NaCl, 2.7mM KCl, 10mM Na_2HPO_4, 1.8mM
748 KH^2PO_4, 20mM N-ethylmaleimide (NEM), pH 7.4). Larval fillet preparations were incubated for 5
749 minutes in PBS-NEM then fixed for 8 minutes in 4% formaldehyde (in PBS-NEM). Specimens were
750 washed three times in PBS-NEM and then equilibrated in 70% glycerol. Specimens were mounted in
751 glycerol and imaged the same day. Imaging was performed on a Leica SP5 point-scanning confocal,

752 using a 63x/1.3 N.A. (Leica) glycerol immersion objective lens. The reporter was excited sequentially
753 at 405nm and 488nm (Albrecht et al., 2011) with emission detected at 500–535nm. 16-bit images
754 were acquired using Leica LAS AF software and processed using ImageJ. Z-stack images were
755 maximally projected and converted to 32-bit. To remove fringing artefacts around bouton edges
756 488nm images were thresholded using the 'Intermodes' algorithm with values below threshold set
757 to 'not a number', and ratio images were created by dividing the 405nm image by the 488nm image
758 pixel by pixel (Albrecht et al., 2011). Regions of Interest were taken on the ratio image spanning the
759 entire NMJ and the mean value obtained from each NMJ was used for statistical analysis.
760
761 **Transmission Electron Microscopy.** Third instar wandering larvae were fillet dissected in PBS and
762 fixed overnight in 0.1M $NaPO_4$, pH 7.4, 1% glutaraldehyde, and 4% formaldehyde, pH 7.3. Fixed
763 specimens were washed 3× in 0.1M $NaPO_4$ before incubation in OsO_4 (1% in 0.1M $NaPO_4$; 2hr).
764 Preparations were washed 3× in distilled water, incubated in 1% uranyl acetate, then washed again
765 (3× distilled water) and dehydrated through a graded ethanol series: 20% increments starting at
766 30% followed by two 100% changes and then 2× 100% propylene oxide. Specimens were incubated
767 in a graded series of epon araldite resin (in propylene oxide): 25% increments culminating in 3×
768 100% changes. Individual muscles were then dissected and transferred into embedding molds,
769 followed by polymerization at 60°C for 48 hrs. Resin mounted specimens were sectioned (60–70
770 nm) using glass knives upon a microtome (Ultracut UCT; Leica). Sections were placed onto grids,
771 incubated in uranyl acetate (50% in ethanol), washed in distilled water and incubated in lead
772 citrate. Sections were imaged using a transmission electron microscope (TECNAI 12 G^2; FEI) with a
773 camera (Soft Imaging Solutions MegaView; Olympus) and Tecnai user interface v2.1.8 and analySIS
774 v3.2 (Soft Imaging Systems).
775
776 **Behavior – larval crawling analysis**
777 To record larval crawling, mid-3rd instar larvae (72hrs ALH) were briefly rinsed in water to remove
778 any food and yeast residues, then up to 12 larvae were placed into a 24cm x 24cm arena of 0.8%
779 agar in water, poured to 5 mm thickness. Crawling behavior was recorded in a temperature and
780 humidity controlled incubator at temperatures ranging from 25-32°C, as indicated for each
781 experiment. Larvae were allowed to acclimatise for 5 minutes, then recorded for 15 minutes under
782 infrared LED illumination (intensity from 14.33 nW/mm^2 in the edge to 9.12 nW/mm^2 in the center),
783 using frustrated total internal reflection using a modified FIM tracker (*36*) https://www.uni-
784 muenster.de/PRIA/en/FIM/index.html. Larvae were recorded with a Basler acA2040-180km CMOS
785 camera using Pylon and StreamPix software, mounted with a 16mm KOWA IJM3sHC.SW VIS-NIR
786 Lens. Images were acquired at 5 frames per second. For each larvae, average crawling speed was
787 calculated from long, uninterrupted forward crawls identified manually using FIMTrack. The 15
788 minute recording period was partitioned into 5 minute sections with each larvae being assayed once
789 within each section, allowing each specimen to be sampled a maximum of 3 times. We observed no
790 change in average crawling speed within the duration of the 15-minute recording.
791
792 **Data Analysis.** All data handling was performed using Prism software (GraphPad). NMJ bouton
793 number and ratiometric ROS reporter data were tested for normal / Gaussian distribution using the
794 D'Agostino-Pearson omnibus normality test. Due to a lower replicate number, dendritic arbor

reconstruction data were tested for normality using the Kolmogorov-Smirnov with Dallal-Wilkinson-Lilliefor P value test. Normal distribution was thus confirmed for all data presented, which were compared using one-way analysis of variance (ANOVA), with Tukey's multiple comparisons test where *P<0.05, **P<0.01, ***P<0.001, ****P<0.0001.

Supplementary Figures

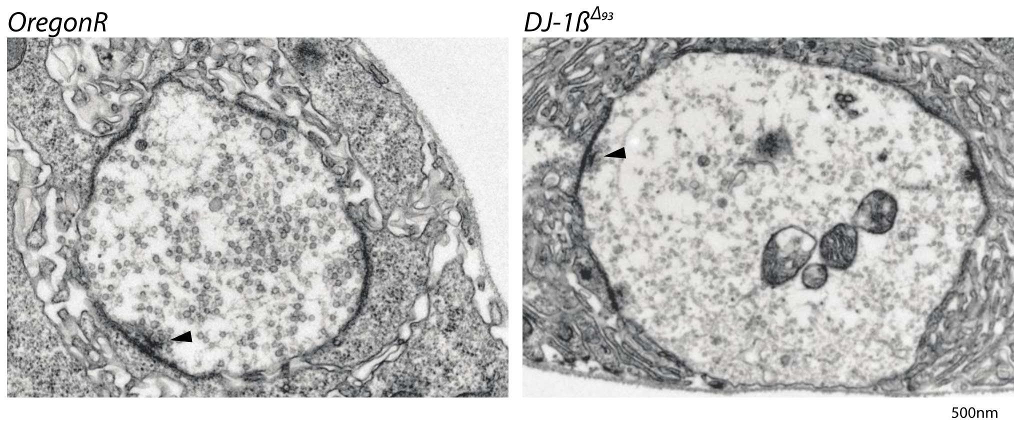

Figure 3-Figure Supplement 1: *DJ-1β*$^{\Delta 93}$ mutant 3rd instar larval NMJs are phenotypically normal. Representative TEM bouton cross-sectional images showing that pre-synaptic architecture is intact including active-zones with associated clustered synaptic vesicles (arrowed).

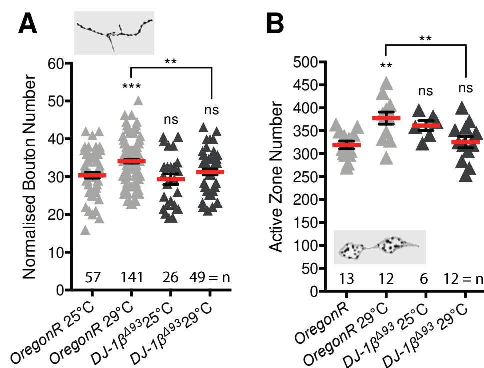

Figure 3-Figure Supplement 2: A. *DJ-1β* null mutant (*DJ-1β*$^{\Delta 93}$) larvae do not show systemic activity-dependent NMJ elaboration. Normalised bouton number dot plot showing significantly increased NMJ elaboration in *OregonR*, but not *DJ-1β*$^{\Delta 93}$, larvae reared at 29°C vs 25°C. **B.** *DJ-1β*$^{\Delta 93}$ larvae also do not show systemic activity-dependent increase in active zone number. *OregonR*, but not *DJ-1β*$^{\Delta 93}$, show significantly increased NMJ active zone number when reared at 29°C vs 25°C. Mean +/- SEM, ANOVA **p<0.01, ***p<0.001, n=replicate number.

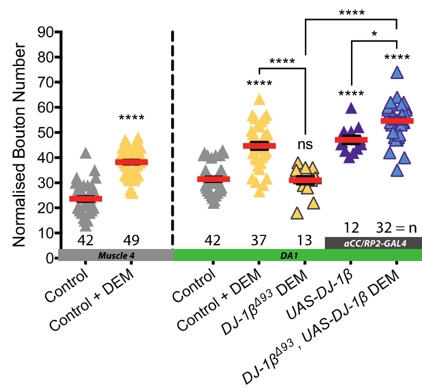

820
821
822 **Figure 3-Figure Supplement 3:** 10mM DEM feeding induces increased bouton number at both
823 muscle 4 and DA1. This response is absent in *DJ-1β* null mutant larvae and is re-established via
824 neuronal (aCC and RP2) specific miss-expression of UAS- *DJ-1β*. UAS- *DJ-1β* expression alone elevates
825 bouton number, which is exacerbated when combined with DEM feeding. Normalised bouton
826 number dot plot, Control is *aCC-FLP-GAL4* alone in heterozygous condition. Mean +/- SEM, ANOVA
827 *p<0.05, ****p<0.0001, n=replicate number.
828

829

830 **References**

831

832 **Adler, V., Yin, Z., Fuchs, S. Y., Benezra, M., Rosario, L., Tew, K. D., Pincus, M. R., Sardana, M.,**
833 **Henderson, C. J., Wolf, C. R., et al.** (1999). Regulation of JNK signaling by GSTp. *EMBO J* **18**,
834 1321–1334.

835 **Albrecht, S. C., Barata, A. G., Grosshans, J., Teleman, A. A. and Dick, T. P.** (2011). In vivo mapping
836 of hydrogen peroxide and oxidized glutathione reveals chemical and regional specificity of redox
837 homeostasis. *Cell Metab* **14**, 819–829.

838 **Ariga, H., Takahashi-Niki, K., Kato, I., Maita, H., Niki, T. and Iguchi-Ariga, S. M. M.** (2013).
839 Neuroprotective function of DJ-1 in Parkinson's disease. *Oxid Med Cell Longev* **2013**, 683920.

840 **Ataman, B., Ashley, J., Gorczyca, M., Ramachandran, P., Fouquet, W., Sigrist, S. J. and Budnik, V.**
841 (2008). Rapid activity-dependent modifications in synaptic structure and function require
842 bidirectional Wnt signaling. *Neuron* **57**, 705–718.

843 **Attwell, D. and Laughlin, S. B.** (2001). An energy budget for signaling in the grey matter of the
844 brain. *J. Cereb. Blood Flow Metab.* **21**, 1133–1145.

845 **Baines, R. A., Robinson, S. G., Fujioka, M., Jaynes, J. B. and Bate, M.** (1999). Postsynaptic
846 expression of tetanus toxin light chain blocks synaptogenesis in Drosophila. *Curr Biol* **9**, 1267–
847 1270.

848 **Baines, R. A., Uhler, J. P., Thompson, A., Sweeney, S. T. and Bate, M.** (2001). Altered electrical
849 properties in Drosophila neurons developing without synaptic transmission. *J Neurosci* **21**,
850 1523–1531.

851 **Bate, M.** (1993). The mesoderm and its derivatives. In *The Development of Drosophila melanogaster*.
852 (eds. Bate, C. M. and Martinez-Arias, A., Cold Spring Harbor: The development of Drosophila
853 melanogaster.

854 **Bayat, V., Jaiswal, M. and Bellen, H. J.** (2011). The BMP signaling pathway at the Drosophila
855 neuromuscular junction and its links to neurodegenerative diseases. *Curr Opin Neurobiol* **21**,
856 182–188.

857 **Bánfi, B., Tirone, F., Durussel, I., Knisz, J., Moskwa, P., Molnár, G. Z., Krause, K.-H. and Cox, J. A.**
858 (2004). Mechanism of Ca2+ activation of the NADPH oxidase 5 (NOX5). *J Biol Chem* **279**, 18583–
859 18591.

860 **Bell, K. F. S., Al-Mubarak, B., Martel, M.-A., Mckay, S., Wheelan, N., Hasel, P., Márkus, N. M.,**
861 **Baxter, P., Deighton, R. F., Serio, A., et al.** (2015). Neuronal development is promoted by
862 weakened intrinsic antioxidant defences due to epigenetic repression of Nrf2. *Nat Comms* **6**,
863 7066.

864 **Berke, B., Wittnam, J., McNeill, E., Van Vactor, D. L. and Keshishian, H.** (2013). Retrograde BMP
865 signaling at the synapse: a permissive signal for synapse maturation and activity-dependent
866 plasticity. *J Neurosci* **33**, 17937–17950.

867 **Bindokas, V. P., Jordán, J., Lee, C. C. and Miller, R. J.** (1996). Superoxide production in rat
868 hippocampal neurons: selective imaging with hydroethidine. *J. Neurosci.* **16**, 1324–1336.

869 **Blackinton, J., Lakshminarasimhan, M., Thomas, K. J., Ahmad, R., Greggio, E., Raza, A. S.,**
870 **Cookson, M. R. and Wilson, M. A.** (2009). Formation of a stabilized cysteine sulfinic acid is
871 critical for the mitochondrial function of the parkinsonism protein DJ-1. *J Biol Chem* **284**, 6476–
872 6485.

873 **Bonifati, V., Rizzu, P., van Baren, M. J., Schaap, O., Breedveld, G. J., Krieger, E., Dekker, M. C. J.,**
874 **Squitieri, F., Ibanez, P., Joosse, M., et al.** (2003). Mutations in the DJ-1 gene associated with
875 autosomal recessive early-onset parkinsonism. *Science* **299**, 256–259.

876 **Brennan, A. M., Won Suh, S., Joon Won, S., Narasimhan, P., Kauppinen, T. M., Lee, H., Edling, Y.,**
877 **Chan, P. H. and Swanson, R. A.** (2009). NADPH oxidase is the primary source of superoxide
878 induced by NMDA receptor activation. *Nat Neurosci* **12**, 857–863.

879 **Brierley, D. J., Blanc, E., Reddy, O. V., VijayRaghavan, K. and Williams, D. W.** (2009). Dendritic
880 targeting in the leg neuropil of Drosophila: the role of midline signalling molecules in generating
881 a myotopic map. *PLoS Biol* **7**, e1000199.

882 **Budnik, V. and Salinas, P. C.** (2011). Wnt signaling during synaptic development and plasticity. *Curr*
883 *Opin Neurobiol* **21**, 151–159.

884 **Calì, T., Ottolini, D., Soriano, M. E. and Brini, M.** (2015). A new split-GFP-based probe reveals DJ-1
885 translocation into the mitochondrial matrix to sustain ATP synthesis upon nutrient deprivation.
886 *Hum Mol Genet* **24**, 1045–1060.

887 **Campbell, M. and Ganetzky, B.** (2012). Extensive morphological divergence and rapid evolution of
888 the larval neuromuscular junction in Drosophila. *Proc Natl Acad Sci U S A*.

889 **Canet-Avilés, R. M. and Wilson, M. A.** (2004). The Parkinson's disease protein DJ-1 is
890 neuroprotective due to cysteine-sulfinic acid-driven mitochondrial localization.

891 **Chandrasekaran, V., Lea, C., Sosa, J. C., Higgins, D. and Lein, P. J.** (2015). Reactive oxygen species
892 are involved in BMP-induced dendritic growth in cultured rat sympathetic neurons. *Mol Cell*
893 *Neurosci* **67**, 116–125.

894 **Cho, R. W., Buhl, L. K., Volfson, D., Tran, A., Li, F., Akbergenova, Y. and Littleton, J. T.** (2015).
895 Phosphorylation of Complexin by PKA Regulates Activity-Dependent Spontaneous
896 Neurotransmitter Release and Structural Synaptic Plasticity. *Neuron* **88**, 749–761.

897 **Choi, J. C., Park, D. and Griffith, L. C.** (2004). Electrophysiological and morphological
898 characterization of identified motor neurons in the Drosophila third instar larva central nervous
899 system. *J Neurophysiol* **91**, 2353–2365.

900 **Chouhan, A. K., Zhang, J., Zinsmaier, K. E. and Macleod, G. T.** (2010). Presynaptic mitochondria in
901 functionally different motor neurons exhibit similar affinities for Ca2+ but exert little influence
902 as Ca2+ buffers at nerve firing rates in situ. *J Neurosci* **30**, 1869–1881.

903 **Crossley, A. C.** (1978). Morphology and development of the Drosophila muscular system. In *Genetics*
904 *and biology of Drosophila* (eds. Ashburner, M. and Wright, T., pp. 499–560. New York: Genetics
905 and biology of Drosophila.

906 **Davis, G. W.** (2006). Homeostatic control of neural activity: from phenomenology to molecular
907 design. *Annu Rev Neurosci* **29**, 307–323.

908 **Davis, G. W. and Müller, M.** (2015). Homeostatic control of presynaptic neurotransmitter release.
909 *Annu Rev Physiol* **77**, 251–270.

910 **Davis, G. W., DiAntonio, A., Petersen, S. A. and Goodman, C. S.** (1998). Postsynaptic PKA controls
911 quantal size and reveals a retrograde signal that regulates presynaptic transmitter release in
912 Drosophila. *Neuron* **20**, 305–315.

913 **Davis, G. W., Schuster, C. M. and Goodman, C. S.** (1996). Genetic dissection of structural and
914 functional components of synaptic plasticity. III. CREB is necessary for presynaptic functional
915 plasticity. *Neuron* **17**, 669–679.

916 **Davydova, D., Marini, C., King, C., Klueva, J., Bischof, F., Romorini, S., Montenegro-Venegas, C.,**
917 **Heine, M., Schneider, R., Schröder, M. S., et al.** (2014). Bassoon specifically controls presynaptic
918 P/Q-type Ca(2+) channels via RIM-binding protein. *Neuron* **82**, 181–194.

919 **Dietzl, G., Chen, D., Schnorrer, F., Su, K.-C., Barinova, Y., Fellner, M., Gasser, B., Kinsey, K.,**
920 **Oppel, S., Scheiblauer, S., et al.** (2007). A genome-wide transgenic RNAi library for conditional
921 gene inactivation in Drosophila. *Nature* **448**, 151–156.

922 **Dillon, M. E., Wang, G., Garrity, P. A. and Huey, R. B.** (2009). Review: Thermal preference in
923 Drosophila. *J. Therm. Biol.* **34**, 109–119.

924 **Do, K. Q., Cuenod, M. and Hensch, T. K.** (2015). Targeting Oxidative Stress and Aberrant Critical
925 Period Plasticity in the Developmental Trajectory to Schizophrenia. *Schizophr Bull* **41**, 835–846.

926 **Driscoll, H. E., Muraro, N. I., He, M. and Baines, R. A.** (2013). Pumilio-2 regulates translation of
927 nav1.6 to mediate homeostasis of membrane excitability. *J Neurosci* **33**, 9644–9654.

928 **Dugan, L. L., Sensi, S. L., Canzoniero, L. M., Handran, S. D., Rothman, S. M., Lin, T. S., Goldberg,**
929 **M. P. and Choi, D. W.** (1995). Mitochondrial production of reactive oxygen species in cortical
930 neurons following exposure to N-methyl-D-aspartate. *J. Neurosci.* **15**, 6377–6388.

931 **Evers, J. F., Schmitt, S., Sibila, M. and Duch, C.** (2005). Progress in functional neuroanatomy:
932 precise automatic geometric reconstruction of neuronal morphology from confocal image
933 stacks. *J Neurophysiol* **93**, 2331–2342.

934 **Finkel, T.** (2011). Signal transduction by reactive oxygen species. *J Cell Biol* **194**, 7–15.

935 **Finkel, T. and Holbrook, N. J.** (2000). Oxidants, oxidative stress and the biology of ageing. *Nature*
936 **408**, 239–247.

937 **Frank, C. A.** (2014). Homeostatic plasticity at the Drosophila neuromuscular junction.
938 *Neuropharmacology* **78**, 63–74.

939 **Frank, C. A., Kennedy, M. J., Goold, C. P., Marek, K. W. and Davis, G. W.** (2006). Mechanisms
940 underlying the rapid induction and sustained expression of synaptic homeostasis. *Neuron* **52**,
941 663–677.

942 **Frank, C. A., Pielage, J. and Davis, G. W.** (2009). A presynaptic homeostatic signaling system
943 composed of the Eph receptor, ephexin, Cdc42, and CaV2.1 calcium channels. *Neuron* **61**, 556–
944 569.

945 **Frank, C. A., Wang, X., Collins, C. A., Rodal, A. A., Yuan, Q., Verstreken, P. and Dickman, D. K.**
946 (2013). New approaches for studying synaptic development, function, and plasticity using
947 Drosophila as a model system. *J Neurosci* **33**, 17560–17568.

948 **Fujioka, M., Lear, B. C., Landgraf, M., Yusibova, G. L., Zhou, J., Riley, K. M., Patel, N. H. and**
949 **Jaynes, J. B.** (2003). Even-skipped, acting as a repressor, regulates axonal projections in
950 Drosophila. *Development* **130**, 5385–5400.

951 **Funato, Y., Michiue, T., Asashima, M. and Miki, H.** (2006). The thioredoxin-related redox-regulating
952 protein nucleoredoxin inhibits Wnt-beta-catenin signalling through dishevelled. *Nat Cell Biol* **8**,
953 501–508.

954 **Fushiki, A., Zwart, M. F., Kohsaka, H., Fetter, R. D., Cardona, A. and Nose, A.** (2016). A circuit
955 mechanism for the propagation of waves of muscle contraction in Drosophila. *Elife* **5**.

956 **Gahtan, E., Auerbach, J. M., Groner, Y. and Segal, M.** (1998). Reversible impairment of long-term
957 potentiation in transgenic Cu/Zn-SOD mice. *Eur J Neurosci* **10**, 538–544.

958 **Gao, X., Neufeld, T. P. and Pan, D.** (2000). Drosophila PTEN regulates cell growth and proliferation
959 through PI3K-dependent and -independent pathways. *Dev Biol* **221**, 404–418.

960 **Gaviño, M. A., Ford, K. J., Archila, S. and Davis, G. W.** (2015). Homeostatic synaptic depression is
961 achieved through a regulated decrease in presynaptic calcium channel abundance. *Elife* **4**.

962 **Giachello, C. N. and Baines, R. A.** (2016). Regulation of motoneuron excitability and the setting of
963 homeostatic limits. *Curr Opin Neurobiol* **43**, 1–6.

964 **Giniatullin, A. R., Darios, F., Shakirzyanova, A., Davletov, B. and Giniatullin, R.** (2006). SNAP25 is
965 a pre-synaptic target for the depressant action of reactive oxygen species on transmitter
966 release. *J Neurochem* **98**, 1789–1797.

967 **Gladyshev, V. N.** (2014). The free radical theory of aging is dead. Long live the damage theory!
968 *Antioxid Redox Signal* **20**, 727–731.

969 **Gutscher, M., Sobotta, M. C., Wabnitz, G. H., Ballikaya, S., Meyer, A. J., Samstag, Y. and Dick, T. P.**
970 (2009). Proximity-based protein thiol oxidation by H2O2-scavenging peroxidases. *J Biol Chem*
971 **284**, 31532–31540.

972 **Ha, E. M.** (2005). A Direct Role for Dual Oxidase in Drosophila Gut Immunity. *Science* **310**, 847–850.

973 **Hallermann, S., de Kock, C. P. J., Stuart, G. J. and Kole, M. H. P.** (2012). State and location
974 dependence of action potential metabolic cost in cortical pyramidal neurons. *Nat Neurosci* **15**,
975 1007–1014.

976 **Halliwell, B.** (1992). Reactive oxygen species and the central nervous system. *J Neurochem* **59**, 1609–
977 1623.

978 **Hamada, F. N., Rosenzweig, M., Kang, K., Pulver, S. R., Ghezzi, A., Jegla, T. J. and Garrity, P. A.**
979 (2008). An internal thermal sensor controlling temperature preference in Drosophila. *Nature*
980 **454**, 217–220.

981 **Hao, L.-Y., Giasson, B. I. and Bonini, N. M.** (2010). DJ-1 is critical for mitochondrial function and
982 rescues PINK1 loss of function. *Proc Natl Acad Sci U S A* **107**, 9747–9752.

983 **HARMAN, D.** (1956). Aging: a theory based on free radical and radiation chemistry. *J Gerontol* **11**,
984 298–300.

985 **Harris, K. P. and Littleton, J. T.** (2015). Transmission, Development, and Plasticity of Synapses.
986 *Genetics* **201**, 345–375.

987 **Hartwig, C. L., Worrell, J., Levine, R. B., Ramaswami, M. and Sanyal, S.** (2008). Normal dendrite
988 growth in Drosophila motor neurons requires the AP-1 transcription factor. *Dev Neurobiol* **68**,
989 1225–1242.

990 **Hoang, B. and Chiba, A.** (2001). Single-cell analysis of Drosophila larval neuromuscular synapses.
991 *Dev Biol* **229**, 55–70.

992 **Hongpaisan, J., Winters, C. A. and Andrews, S. B.** (2004). Strong calcium entry activates
993 mitochondrial superoxide generation, upregulating kinase signaling in hippocampal neurons. *J*
994 *Neurosci* **24**, 10878–10887.

995 **Höhn, A. and Grune, T.** (2013). Lipofuscin: formation, effects and role of macroautophagy. *Redox*
996 *Biol* **1**, 140–144.

997 **Huddleston, A. T., Tang, W., Takeshima, H., Hamilton, S. L. and Klann, E.** (2008). Superoxide-
998 induced potentiation in the hippocampus requires activation of ryanodine receptor type 3 and
999 ERK. *J Neurophysiol* **99**, 1565–1571.

1000 **Itakura, Y., Kohsaka, H., Ohyama, T., Zlatic, M., Pulver, S. R. and Nose, A.** (2015). Identification of
1001 Inhibitory Premotor Interneurons Activated at a Late Phase in a Motor Cycle during Drosophila
1002 Larval Locomotion. *PLoS ONE* **10**, e0136660.

1003 **Jindra, M., Gaziova, I., Uhlirova, M., Okabe, M., Hiromi, Y. and Hirose, S.** (2004). Coactivator
1004 MBF1 preserves the redox-dependent AP-1 activity during oxidative stress in Drosophila. *EMBO*
1005 *J* **23**, 3538–3547.

1006 **Jordán-Álvarez, S., Fouquet, W., Sigrist, S. J. and Acebes, A.** (2012). Presynaptic PI3K activity
1007 triggers the formation of glutamate receptors at neuromuscular terminals of Drosophila. *J Cell*
1008 *Sci* **125**, 3621–3629.

1009 **Kamsler, A. and Segal, M.** (2003a). Hydrogen peroxide modulation of synaptic plasticity. *J Neurosci*
1010 **23**, 269–276.

1011 **Kamsler, A. and Segal, M.** (2003b). Paradoxical actions of hydrogen peroxide on long-term
1012 potentiation in transgenic superoxide dismutase-1 mice. *J Neurosci* **23**, 10359–10367.

1013 **Kim, R. H., Peters, M., Jang, Y., Shi, W., Pintilie, M., Fletcher, G. C., DeLuca, C., Liepa, J., Zhou, L.,**
1014 **Snow, B., et al.** (2005). DJ-1, a novel regulator of the tumor suppressor PTEN. *Cancer Cell* **7**,
1015 263–273.

1016 **Kim, S. M., Kumar, V., Lin, Y. Q., Karunanithi, S. and Ramaswami, M.** (2009a). Fos and Jun
1017 potentiate individual release sites and mobilize the reserve synaptic vesicle pool at the
1018 Drosophila larval motor synapse. *Proc Natl Acad Sci U S A* **106**, 4000–4005.

1019 **Kim, Y.-C., Kitaura, H., Taira, T., Iguchi-Ariga, S. M. M. and Ariga, H.** (2009b). Oxidation of DJ-1-
1020 dependent cell transformation through direct binding of DJ-1 to PTEN. *Int J Oncol* **35**, 1331–
1021 1341.

1022 **Kishida, K. T., Hoeffer, C. A., Hu, D., Pao, M., Holland, S. M. and Klann, E.** (2006). Synaptic
1023 plasticity deficits and mild memory impairments in mouse models of chronic granulomatous
1024 disease. *Mol Cell Biol* **26**, 5908–5920.

1025 **Klann, E.** (1998). Cell-permeable scavengers of superoxide prevent long-term potentiation in
1026 hippocampal area CA1. *J Neurophysiol* **80**, 452–457.

1027 **Knapp, L. T. and Klann, E.** (2002). Potentiation of hippocampal synaptic transmission by superoxide
1028 requires the oxidative activation of protein kinase C. *J Neurosci* **22**, 674–683.

1029 **Kohsaka, H., Okusawa, S., Itakura, Y., Fushiki, A. and Nose, A.** (2012). Development of larval
1030 motor circuits in Drosophila. *Dev Growth Differ* **54**, 408–419.

1031 **Kohsaka, H., Takasu, E., Morimoto, T. and Nose, A.** (2014). A group of segmental premotor
1032 interneurons regulates the speed of axial locomotion in Drosophila larvae. *Curr Biol* **24**, 2632–
1033 2642.

1034 **Koles, K. and Budnik, V.** (2012). Wnt signaling in neuromuscular junction development. *Cold Spring*
1035 *Harb Perspect Biol* **4**.

1036 **Landgraf, M., Jeffrey, V., Fujioka, M., Jaynes, J. B. and Bate, M.** (2003). Embryonic origins of a
1037 motor system: motor dendrites form a myotopic map in Drosophila. *PLoS Biol* **1**, E41.

1038 **Lazarevic, V., Schöne, C., Heine, M., Gundelfinger, E. D. and Fejtova, A.** (2011). Extensive
1039 remodeling of the presynaptic cytomatrix upon homeostatic adaptation to network activity
1040 silencing. *J Neurosci* **31**, 10189–10200.

1041 **Lee, K. Y., Chung, K. and Chung, J. M.** (2010). Involvement of reactive oxygen species in long-term
1042 potentiation in the spinal cord dorsal horn. *J Neurophysiol* **103**, 382–391.

1043 **Leevers, S. J., Weinkove, D., MacDougall, L. K., Hafen, E. and Waterfield, M. D.** (1996). The
1044 Drosophila phosphoinositide 3-kinase Dp110 promotes cell growth. *EMBO J* **15**, 6584–6594.

1045 **Levin, E. D., Brady, T. C., Hochrein, E. C., Oury, T. D., Jonsson, L. M., Marklund, S. L. and Crapo, J.**
1046 **D.** (1998). Molecular manipulations of extracellular superoxide dismutase: functional
1047 importance for learning. *Behav. Genet.* **28**, 381–390.

1048 **Liemburg-Apers, D. C., Willems, P. H. G. M., Koopman, W. J. H. and Grefte, S.** (2015). Interactions
1049 between mitochondrial reactive oxygen species and cellular glucose metabolism. *Arch. Toxicol.*
1050 **89**, 1209–1226.

1051 **Lin, J., Prahlad, J. and Wilson, M. A.** (2012a). Conservation of oxidative protein stabilization in an
1052 insect homologue of parkinsonism-associated protein DJ-1. *Biochemistry* **51**, 3799–3807.

1053 **Lin, W.-H., Günay, C., Marley, R., Prinz, A. A. and Baines, R. A.** (2012b). Activity-dependent
1054 alternative splicing increases persistent sodium current and promotes seizure. *J Neurosci* **32**,
1055 7267–7277.

1056 **Loebrich, S. and Nedivi, E.** (2009). The function of activity-regulated genes in the nervous system.
1057 *Physiol Rev* **89**, 1079–1103.

1058 **Love, N. R., Chen, Y., Ishibashi, S., Kritsiligkou, P., Lea, R., Koh, Y., Gallop, J. L., Dorey, K. and**
1059 **Amaya, E.** (2013). Amputation-induced reactive oxygen species are required for successful
1060 Xenopus tadpole tail regeneration. *Nat Cell Biol*.

1061 **Luo, J., Shen, W. L. and Montell, C.** (2016). TRPA1 mediates sensation of the rate of temperature
1062 change in Drosophila larvae. *Nat Neurosci*.

1063 **Marrus, S. B. and DiAntonio, A.** (2005). Investigating the safety factor at an invertebrate
1064 neuromuscular junction. *J Neurobiol* **63**, 62–69.

1065 **Martins, R. N., Harper, C. G., Stokes, G. B. and Masters, C. L.** (1986). Increased cerebral glucose-6-
1066 phosphate dehydrogenase activity in Alzheimer's disease may reflect oxidative stress. *J*
1067 *Neurochem* **46**, 1042–1045.

1068 **Martín-Peña, A., Acebes, A., Rodríguez, J.-R., Sorribes, A., de Polavieja, G. G., Fernández-Fúnez,**
1069 **P. and Ferrús, A.** (2006). Age-independent synaptogenesis by phosphoinositide 3 kinase. *J*
1070 *Neurosci* **26**, 10199–10208.

1071 **Massaad, C. A. and Klann, E.** (2011). Reactive oxygen species in the regulation of synaptic plasticity
1072 and memory. *Antioxid Redox Signal* **14**, 2013–2054.

1073 **Matz, J., Gilyan, A., Kolar, A., McCarvill, T. and Krueger, S. R.** (2010). Rapid structural alterations
1074 of the active zone lead to sustained changes in neurotransmitter release. *Proc Natl Acad Sci U S*
1075 *A* **107**, 8836–8841.

1076 **Mauss, A., Tripodi, M., Evers, J. F. and Landgraf, M.** (2009). Midline signalling systems direct the
1077 formation of a neural map by dendritic targeting in the Drosophila motor system. *PLoS Biol* **7**,
1078 e1000200.

1079 **Mee, C. J., Pym, E. C. G., Moffat, K. G. and Baines, R. A.** (2004). Regulation of neuronal excitability
1080 through pumilio-dependent control of a sodium channel gene. *J Neurosci* **24**, 8695–8703.

1081 **Meulener, M. C., Xu, K., Thomson, L., Thompson, L., Ischiropoulos, H. and Bonini, N. M.** (2006).
1082 Mutational analysis of DJ-1 in Drosophila implicates functional inactivation by oxidative damage
1083 and aging. *Proc Natl Acad Sci USA* **103**, 12517–12522.

1084 **Meulener, M., Whitworth, A. J., Armstrong-Gold, C. E., Rizzu, P., Heutink, P., Wes, P. D., Pallanck,**
1085 **L. J. and Bonini, N. M.** (2005). Drosophila DJ-1 mutants are selectively sensitive to
1086 environmental toxins associated with Parkinson's disease. *Curr Biol* **15**, 1572–1577.

1087 **Milton, V. J. and Sweeney, S. T.** (2012). Oxidative stress in synapse development and function. *Dev*
1088 *Neurobiol* **72**, 100–110.

1089 **Milton, V. J., Jarrett, H. E., Gowers, K., Chalak, S., Briggs, L., Robinson, I. M. and Sweeney, S. T.**
1090 (2011). Oxidative stress induces overgrowth of the Drosophila neuromuscular junction. *Proc Natl*
1091 *Acad Sci U S A* **108**, 17521–17526.

1092 **Missirlis, F., Phillips, J. P. and Jäckle, H.** (2001). Cooperative action of antioxidant defense systems
1093 in Drosophila. *Current Biology* **11**, 1272–1277.

1094 **Missirlis, F., Rahlfs, S., Dimopoulos, N., Bauer, H., Becker, K., Hilliker, A., Phillips, J. P. and Jäckle,**
1095 **H.** (2003). A putative glutathione peroxidase of Drosophila encodes a thioredoxin peroxidase
1096 that provides resistance against oxidative stress but fails to complement a lack of catalase
1097 activity. *Biol Chem* **384**, 463–472.

1098 **Munnamalai, V. and Suter, D. M.** (2009). Reactive oxygen species regulate F-actin dynamics in
1099 neuronal growth cones and neurite outgrowth. *J Neurochem* **108**, 644–661.

1100 **Munnamalai, V., Weaver, C. J., Weisheit, C. E., Venkatraman, P., Agim, Z. S., Quinn, M. T. and**
1101 **Suter, D. M.** (2014). Bidirectional interactions between NOX2-type NADPH oxidase and the F-
1102 actin cytoskeleton in neuronal growth cones. *J Neurochem* **130**, 526–540.

1103 **Müller, M. and Davis, G. W.** (2012). Transsynaptic control of presynaptic Ca^{2+} influx achieves
1104 homeostatic potentiation of neurotransmitter release. *Curr Biol* **22**, 1102–1108.

1105 **Nagakubo, D., Taira, T., Kitaura, H., Ikeda, M., Tamai, K., Iguchi-Ariga, S. M. and Ariga, H.** (1997).
1106 DJ-1, a novel oncogene which transforms mouse NIH3T3 cells in cooperation with ras. *Biochem*
1107 *Biophys Res Commun* **231**, 509–513.

1108 **O'Leary, T., Williams, A. H., Caplan, J. S. and Marder, E.** (2013). Correlations in ion channel
1109 expression emerge from homeostatic tuning rules. *Proc Natl Acad Sci U S A* **110**, E2645–54.

1110 **Olguín-Albuerne, M. and Morán, J.** (2015). ROS produced by NOX2 control in vitro development of
1111 cerebellar granule neurons development. *ASN Neuro* **7**.

1112 **Osses, N. and Henriquez, J. P.** (2014). Bone morphogenetic protein signaling in vertebrate motor
1113 neurons and neuromuscular communication. *Front Cell Neurosci* **8**, 453.

1114 **Ou, Y., Chwalla, B., Landgraf, M. and van Meyel, D. J.** (2008). Identification of genes influencing
1115 dendrite morphogenesis in developing peripheral sensory and central motor neurons. *Neural*
1116 *development* **3**, 16.

1117 **Owald, D., Lin, S. and Waddell, S.** (2015). Light, heat, action: neural control of fruit fly behaviour.
1118 *Philos Trans R Soc Lond, B, Biol Sci* **370**, 20140211.

1119 **Pandey, D., Gratton, J.-P., Rafikov, R., Black, S. M. and Fulton, D. J. R.** (2011). Calcium/calmodulin-
1120 dependent kinase II mediates the phosphorylation and activation of NADPH oxidase 5. *Mol.*
1121 *Pharmacol.* **80**, 407–415.

1122 **Peled, E. S., Newman, Z. L. and Isacoff, E. Y.** (2014). Evoked and spontaneous transmission favored
1123 by distinct sets of synapses. *Curr Biol* **24**, 484–493.

1124 **Peng, T.-I. and Jou, M.-J.** (2010). Oxidative stress caused by mitochondrial calcium overload. *Ann N*
1125 *Y Acad Sci* **1201**, 183–188.

1126 **Piccioli, Z. D. and Littleton, J. T.** (2014). Retrograde BMP Signaling Modulates Rapid Activity-
1127 Dependent Synaptic Growth via Presynaptic LIM Kinase Regulation of Cofilin. *J Neurosci* **34**,
1128 4371–4381.

1129 **Prinz, A. A.** (2006). Insights from models of rhythmic motor systems. *Curr Opin Neurobiol* **16**, 615–
1130 620.

1131 **Prinz, A. A., Bucher, D. and Marder, E.** (2004). Similar network activity from disparate circuit
1132 parameters. *Nat Neurosci* **7**, 1345–1352.

1133 **Pulver, S. R., Pashkovski, S. L., Hornstein, N. J., Garrity, P. A. and Griffith, L. C.** (2009). Temporal
1134 dynamics of neuronal activation by Channelrhodopsin-2 and TRPA1 determine behavioral
1135 output in Drosophila larvae. *J Neurophysiol* **101**, 3075–3088.

1136 **Rharass, T., Lemcke, H., Lantow, M., Kuznetsov, S. A., Weiss, D. G. and Panáková, D.** (2014).
1137 Ca2+-mediated mitochondrial reactive oxygen species metabolism augments Wnt/β-catenin
1138 pathway activation to facilitate cell differentiation. *J Biol Chem* **289**, 27937–27951.

1139 **Rosenzweig, M., Brennan, K. M., Tayler, T. D., Phelps, P. O., Patapoutian, A. and Garrity, P. A.**
1140 (2005). The Drosophila ortholog of vertebrate TRPA1 regulates thermotaxis. *Genes Dev* **19**, 419–
1141 424.

1142 **Roy, B., Singh, A. P., Shetty, C., Chaudhary, V., North, A., Landgraf, M., VijayRaghavan, K. and**
1143 **Rodrigues, V.** (2007). Metamorphosis of an identified serotonergic neuron in the Drosophila
1144 olfactory system. *Neural development* **2**, 20.

1145 **Saitoh, M., Nishitoh, H., Fujii, M., Takeda, K., Tobiume, K., Sawada, Y., Kawabata, M., Miyazono,**
1146 **K. and Ichijo, H.** (1998). Mammalian thioredoxin is a direct inhibitor of apoptosis signal-
1147 regulating kinase (ASK) 1. *EMBO J* **17**, 2596–2606.

1148 **Sanyal, S., Narayanan, R., Consoulas, C. and Ramaswami, M.** (2003). Evidence for cell
1149 autonomous AP1 function in regulation of Drosophila motor-neuron plasticity. *BMC neuroscience*
1150 **4**, 20.

1151 **Sanyal, S., Sandstrom, D. J., Hoeffer, C. A. and Ramaswami, M.** (2002). AP-1 functions upstream of
1152 CREB to control synaptic plasticity in Drosophila. *Nature* **416**, 870–874.

1153 **Schmitt, S., Evers, J. F., Duch, C., Scholz, M. and Obermayer, K.** (2004). New methods for the
1154 computer-assisted 3-D reconstruction of neurons from confocal image stacks. *Neuroimage* **23**,
1155 1283–1298.

1156 **Schneider-Mizell, C. M., Gerhard, S., Longair, M., Kazimiers, T., Li, F., Zwart, M. F., Champion, A.,**
1157 **Midgley, F. M., Fetter, R. D., Saalfeld, S., et al.** (2016). Quantitative neuroanatomy for
1158 connectomics in Drosophila. *Elife* **5**.

1159 **Serrano, F., Kolluri, N. S., Wientjes, F. B., Card, J. P. and Klann, E.** (2003). NADPH oxidase
1160 immunoreactivity in the mouse brain. *Brain Res* **988**, 193–198.

1161 **Shearin, H. K., Macdonald, I. S., Spector, L. P. and Stowers, R. S.** (2014). Hexameric GFP and
1162 mCherry Reporters for the Drosophila GAL4, Q, and LexA Transcription Systems. *Genetics* **196**,
1163 951–960.

1164 **Sigrist, S. J., Reiff, D. F., Thiel, P. R., Steinert, J. R. and Schuster, C. M.** (2003). Experience-
1165 dependent strengthening of Drosophila neuromuscular junctions. *J Neurosci* **23**, 6546–6556.

1166 **Sink, H. and Whitington, P. M.** (1991). Location and connectivity of abdominal motoneurons in the
1167 embryo and larva of Drosophila melanogaster. *J Neurobiol* **22**, 298–311.

1168 **Sorce, S., Stocker, R., Seredenina, T., Holmdahl, R., Aguzzi, A., Chio, A., Depaulis, A., Heitz, F.,**
1169 **Olofsson, P., Olsson, T., et al.** (2017). NADPH oxidases as drug targets and biomarkers in
1170 neurodegenerative diseases: What is the evidence? *Free Radic Biol Med* **112**, 387–396.

1171 **Soriano, F. X., Baxter, P., Murray, L. M., Sporn, M. B., Gillingwater, T. H. and Hardingham, G. E.**
1172 (2009). Transcriptional regulation of the AP-1 and Nrf2 target gene sulfiredoxin. *Mol. Cells* **27**,
1173 279–282.

1174 **Spina, M. B. and Cohen, G.** (1989). Dopamine turnover and glutathione oxidation: implications for
1175 Parkinson disease. *Proc Natl Acad Sci USA* **86**, 1398–1400.

1176 **Steullet, P., Cabungcal, J.-H., Coyle, J., Didriksen, M., Gill, K., Grace, A. A., Hensch, T. K.,**
1177 **LaMantia, A.-S., Lindemann, L., Maynard, T. M., et al.** (2017). Oxidative stress-driven
1178 parvalbumin interneuron impairment as a common mechanism in models of schizophrenia. *Mol.*
1179 *Psychiatry* **22**, 936–943.

1180 **Stewart, B. A., Atwood, H. L., Renger, J. J., Wang, J. and Wu, C. F.** (1994). Improved stability of
1181 Drosophila larval neuromuscular preparations in haemolymph-like physiological solutions. *J*
1182 *Comp Physiol A* **175**, 179–191.

1183 **Stuart, J. A., Maddalena, L. A., Merilovich, M. and Robb, E. L.** (2014). A midlife crisis for the
1184 mitochondrial free radical theory of aging. *Longev Healthspan* **3**, 4.

1185 **Sugie, A., Hakeda-Suzuki, S., Suzuki, E., Silies, M., Shimozono, M., Möhl, C., Suzuki, T. and**
1186 **Tavosanis, G.** (2015). Molecular Remodeling of the Presynaptic Active Zone of Drosophila
1187 Photoreceptors via Activity-Dependent Feedback. *Neuron* **86**, 711–725.

1188 **Sulkowski, M., Kim, Y.-J. and Serpe, M.** (2014). Postsynaptic glutamate receptors regulate local
1189 BMP signaling at the Drosophila neuromuscular junction. *Development* **141**, 436–447.

1190 **Tejada-Simon, M. V., Serrano, F., Villasana, L. E., Kanterewicz, B. I., Wu, G. Y., Quinn, M. T. and**
1191 **Klann, E.** (2005). Synaptic localization of a functional NADPH oxidase in the mouse
1192 hippocampus. *Molecular and Cellular Neuroscience* **29**, 97–106.

1193 **Thiels, E., Urban, N. N., Gonzalez-Burgos, G. R., Kanterewicz, B. I., Barrionuevo, G., Chu, C. T.,**
1194 **Oury, T. D. and Klann, E.** (2000). Impairment of long-term potentiation and associative
1195 memory in mice that overexpress extracellular superoxide dismutase. *J Neurosci* **20**, 7631–7639.

1196 **Tirone, F. and Cox, J. A.** (2007). NADPH oxidase 5 (NOX5) interacts with and is regulated by
1197 calmodulin. *FEBS Lett* **581**, 1202–1208.

1198 **Tonks, N. K.** (2005). Redox redux: revisiting PTPs and the control of cell signaling. *Cell* **121**, 667–670.

1199 **Tonks, N. K.** (2006). Protein tyrosine phosphatases: from genes, to function, to disease. *Nat Rev Mol*
1200 *Cell Biol* **7**, 833–846.

1201 **Tripodi, M., Evers, J. F., Mauss, A., Bate, M. and Landgraf, M.** (2008). Structural homeostasis:
1202 compensatory adjustments of dendritic arbor geometry in response to variations of synaptic
1203 input. *PLoS Biol* **6**, e260.

1204 **Tsai, P.-I., Wang, M., Kao, H.-H., Cheng, Y.-J., Lin, Y.-J., Chen, R.-H. and Chien, C.-T.** (2012).
1205 Activity-dependent retrograde laminin A signaling regulates synapse growth at Drosophila
1206 neuromuscular junctions. *Proc Natl Acad Sci U S A* **109**, 17699–17704.

1207 **Ueda, A. and Wu, C.-F.** (2015). The role of cAMP in synaptic homeostasis in response to
1208 environmental temperature challenges and hyperexcitability mutations. *Front Cell Neurosci* **9**,
1209 10.

1210 **Waak, J., Weber, S. S., Görner, K., Schall, C., Ichijo, H., Stehle, T. and Kahle, P. J.** (2009). Oxidizable
1211 residues mediating protein stability and cytoprotective interaction of DJ-1 with apoptosis signal-
1212 regulating kinase 1. *J Biol Chem* **284**, 14245–14257.

1213 **Wagh, D. A., Rasse, T. M., Asan, E., Hofbauer, A., Schwenkert, I., Dürrbeck, H., Buchner, S.,**
1214 **Dabauvalle, M.-C., Schmidt, M. and Qin, G.** (2006). Bruchpilot, a Protein with Homology to

1215 ELKS/CAST, Is Required for Structural Integrity and Function of Synaptic Active Zones in
1216 Drosophila. *Neuron* **49**, 833–844.

1217 **Walker, J. A., Gouzi, J. Y., Long, J. B., Huang, S., Maher, R. C., Xia, H., Khalil, K., Ray, A., Van**
1218 **Vactor, D., Bernards, R., et al.** (2013). Genetic and Functional Studies Implicate Synaptic
1219 Overgrowth and Ring Gland cAMP/PKA Signaling Defects in the Drosophila melanogaster
1220 Neurofibromatosis-1 Growth Deficiency. *PLoS Genet* **9**, e1003958.

1221 **Wang, T., Hauswirth, A. G., Tong, A., Dickman, D. K. and Davis, G. W.** (2014). Endostatin Is a
1222 Trans-Synaptic Signal for Homeostatic Synaptic Plasticity. *Neuron*.

1223 **Weyhersmüller, A., Hallermann, S., Wagner, N. and Eilers, J.** (2011). Rapid active zone remodeling
1224 during synaptic plasticity. *J Neurosci* **31**, 6041–6052.

1225 **Wilson, C., Muñoz-Palma, E., Henríquez, D. R., Palmisano, I., Núñez, M. T., Di Giovanni, S. and**
1226 **González-Billault, C.** (2016). A Feed-Forward Mechanism Involving the NOX Complex and RyR-
1227 Mediated Ca2+ Release During Axonal Specification. *J Neurosci* **36**, 11107–11119.

1228 **Wilson, C., Núñez, M. T. and González-Billault, C.** (2015). Contribution of NADPH oxidase to the
1229 establishment of hippocampal neuronal polarity in culture. *J Cell Sci* **128**, 2989–2995.

1230 **Wolfram, V. and Baines, R. A.** (2013). Blurring the boundaries: developmental and activity-
1231 dependent determinants of neural circuits. *Trends Neurosci*.

1232 **Yeates, C. J., Zwiefelhofer, D. J. and Frank, C. A.** (2017). The Maintenance of Synaptic Homeostasis
1233 at the Drosophila Neuromuscular Junction Is Reversible and Sensitive to High Temperature.
1234 *eNeuro* **4**, ENEURO.0220–17.2017.

1235 **Younger, M. A., Müller, M., Tong, A., Pym, E. C. and Davis, G. W.** (2013). A presynaptic ENaC
1236 channel drives homeostatic plasticity. *Neuron* **79**, 1183–1196.

1237 **Zhong, Y. and Wu, C.-F.** (2004). Neuronal Activity and Adenylyl Cyclase in Environment-Dependent
1238 Plasticity of Axonal Outgrowth in Drosophila. *J Neurosci* **24**, 1439–1445.

1239 **Zhu, X.-H., Qiao, H., Du, F., Xiong, Q., Liu, X., Zhang, X., Ugurbil, K. and Chen, W.** (2012).
1240 Quantitative imaging of energy expenditure in human brain. *Neuroimage* **60**, 2107–2117.

1241 **Zwart, M. F., Pulver, S. R., Truman, J. W., Fushiki, A., Fetter, R. D., Cardona, A. and Landgraf, M.**
1242 (2016). Selective Inhibition Mediates the Sequential Recruitment of Motor Pools. *Neuron* **91**,
1243 944.

1244 **Zwart, M. F., Randlett, O., Evers, J. F. and Landgraf, M.** (2013). Dendritic growth gated by a steroid
1245 hormone receptor underlies increases in activity in the developing Drosophila locomotor
1246 system. *Proc Natl Acad Sci U S A*.

1247

1248

1249